WATER RESOURCES RESEARCH, VOL. 49, 1–18, doi:10.1029/2012WR012379, 2013

An unmixing algorithm for remotely sensed soil moisture

Amor V. M. Ines,[1,2] Binayak P. Mohanty,[1] and Yongchul Shin[1]

Received 10 May 2012; revised 12 December 2012; accepted 12 December 2012.

[1] We present an unmixing method, based on genetic algorithm-soil-vegetation-atmosphere-transfer modeling to extract subgrid information of soil and vegetation from remotely sensed soil moisture (downscaled; e.g., soil hydraulic properties, area fractions of soil-vegetation combinations, and unmixed soil moisture time series) that most land surface models use. The unmixing method was evaluated using numerical experiments comprising mixed pixels with simple and complex soil-vegetation combinations, in idealized case studies (with or without uncertainty) and under actual field conditions (Walnut Creek (WC11) field, Soil Moisture Experiment 2005, Iowa). Additional validation experiments were conducted at an airborne-remote sensing footprint (Little Washita (LW21) site, Southern Great Plains 1997 hydrology campaign, Oklahoma) using Electronically Scanning Thin Array Radiometer (ESTAR). Results of the idealized experiments suggest that the unmixing method can extract optimal or near-optimal solutions to the inverse problem under different hydrologic and climatic conditions. Errors in soil moisture data and initial and boundary conditions can compound uncertainty in the solution. The solutions generated under actual field conditions (WC11 field) were able to match soil moisture observations. Analysis showed that typical soil moisture retention curves of cataloged dominant soils in WC11 field did not match well with the measurements, but those derived from actual field-scale soil moisture inversion matched better. The unmixing method performed well in replicating soil hydraulic behavior at the ESTAR footprint. Unlike in WC11 field, the typical soil moisture retention curves of cataloged soils in LW21 field matched better with the measurements. We envisaged that the unmixing method can provide quick and easy way of extracting subgrid soil moisture variability and soil-vegetation information in a pixel.

Citation: Ines, A. V. M., B. P. Mohanty, and Y. Shin (2013), An unmixing algorithm for remotely sensed soil moisture, *Water Resour. Res.*, *49*, doi:10.1029/2012WR012379.

1. Introduction

[2] Soil moisture is critical for many applications in agriculture, hydrology, and climate. Thus, its measurement at different (spatial) scales (from point, field to remote sensing (RS) footprint) is important to better understand soil moisture dynamics at the critical zone [*Brantley et al*., 2006] and develop sustainable ways on how to use and manage our land and water resources.

[3] Soil moisture is measured in the field using direct or indirect methods. However, point-scale observations have small spatial extent that their uses in large-scale applications are rather limited [*Hollinger and Isard*, 1994; *Robock et al*., 2000]. RS has paved the way for measuring soil moisture at larger scales resulting to availability of global soil moisture products (e.g., Advanced Microwave Scanning Radiometer–EOS, Soil Moisture and Ocean Salinity, advanced scatterometer, and Soil Moisture Active Passive, in the near future) that can be used for various applications [*Kerr et al*., 2001; *Njoku et al*., 2003; *Jackson et al*., 2005a, 2005b; *Bartalis et al*., 2008; *Entekhabi et al*., 2010; *Das et al*., 2011]. RS soil moisture has been used to initialize soil-vegetation-atmosphere-transfer (SVAT) models and climate models [e.g., *Das and Mohanty*, 2006; *Ni-Meister et al*., 2006], to estimate soil hydraulic properties for large-scale hydroclimatic applications [e.g., *Ines and Mohanty*, 2008a, 2009], in agricultural and water management [e.g., *Scott et al*., 2003], among others.

[4] Apparently, soil moisture data from airborne/satellite platforms are very promising to support large-scale applications because of their spatial and temporal extents [*Kerr et al*., 2001; *Njoku et al*., 2003; *Entekhabi et al*., 2010; *Das et al*., 2011]. However, to realize their fullest potential, it is necessary to downscale to the highest possible resolution [e.g., *Merlin et al*., 2008; *Das et al*., 2011]. Note however that there is a limit of how far we can downscale RS soil moisture, and after downscaling we can expect still aggregate information in the pixel. Many land surface models used for decision support require this subgrid information about the soil and vegetation to estimate better fluxes. Quantifying such subgrid information from RS soil moisture is therefore important but entails the development of

[1]Department of Biological and Agricultural Engineering, Texas A&M University, College Station, Texas, USA.
[2]Now at International Research Institute for Climate and Society, The Earth Institute at Columbia University, Palisades, New York, USA.

Corresponding author: B. P. Mohanty, Department of Biological and Agricultural Engineering, Texas A&M University, 2117 TAMU, 201 Scoates Hall, College Station, TX 77843, USA. (bmohanty@tamu.edu)

0043-1397/13/2012WR012379

efficient unmixing algorithms capable of performing unmixing of soil moisture at different spatial extents, including satellite data at the global scale.

[5] In this paper, we present an unmixing method based on a combined simulation-optimization scheme, using an integrated inverse Soil-Water-Atmosphere-Plant (SWAP) model and genetic algorithm (GA), that aims to extract value-added information from RS soil moisture data, e.g., subgrid soil moisture, effective soil hydraulic properties, and soil and vegetation fractions. The method was evaluated and validated using (i) idealized numerical studies and (ii) actual field-scale case studies at Walnut Creek (WC) watershed, Iowa, during the Soil Moisture Experiment 2005 (SMEX05) campaign and at an airborne-RS footprint in Little Washita (LW) watershed, Oklahoma, during the Southern Great Plains 1997 (SGP97) hydrology experiments.

2. Materials and Methods

2.1. Mixed-Pixel Model

[6] Let us consider a simple mixed pixel (flat surface) containing three soils similar to the modeling domain presented in Figure 1 but containing one vegetation only (uniform cover). We can write the mixed near-surface soil moisture in the pixel for a period of time as follows:

$$\overline{\theta}_t(\boldsymbol{k}) = \sum_{i=1}^{N} a_i \theta_{it} + e_t, \qquad \forall t, \tag{1}$$

where $\overline{\theta}(\boldsymbol{k})$ ($cm^3\ cm^{-3}$) is the approximated pixel-based near-surface soil moisture for given $\boldsymbol{k}$, a_i (–) stands for the area fraction of soil i in the pixel, θ_i ($cm^3\ cm^{-3}$) is the representative local-scale near-surface soil moisture at soil i, N (=3) is the number of soil types encompassed within a pixel, t is the index for time, and e_t is an error term. Terms inside the summation operator at the right-hand side of equation 1 are called the scaled (weighted) near-surface soil moistures indicating the contributions of particular soil types to the resultant pixel-based soil moisture. The variable $\boldsymbol{k}$, termed unmixing variable, is defined by $\boldsymbol{k} = \left\{\boldsymbol{s}_{i=1,\ldots,N}, a_{i=1,\ldots,N}\right\}$, where $\boldsymbol{s}_i$ component is an array of effective soil hydraulic properties for soil i contained within the pixel, and a_i is the area fraction of soil i as defined above. The components of $\boldsymbol{k}$ are considered to be the most sensitive parameters influencing the resultant pixel-based soil moisture. In reality, however, there are other sources of soil moisture variability, e.g., topography and rainfall gradients. Topography affects soil moisture variability due to its influence on rainwater movement across the landscape: valley is wetter than hilltop, whereas hillslope is intermediate. Rainfall gradient controls soil moisture variation across the landscape, if not considered could lead to model bias when station rainfall did not capture the extent of rainfall event. In this study, we limited our scope to soil and vegetation affecting soil moisture variability in a flat surface.

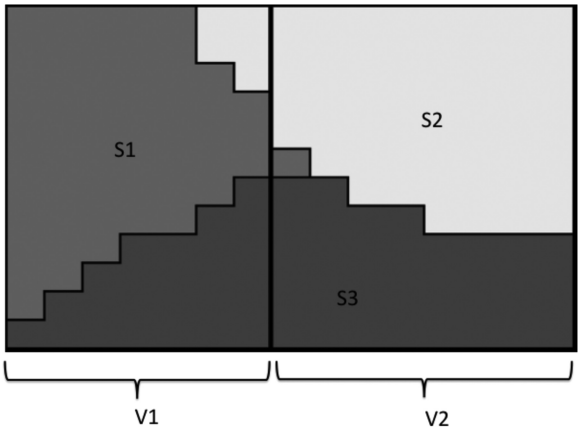

Figure 1. Hypothetical modeling domain (three soils and two vegetations) used in the numerical experiments. *Note*: s_1, soil1; s_2, soil2; s_3, soil3; v_1, vegetation 1; v_2, vegetation 2.

[7] Let the Mualem-Van Genuchten functions [*Van Genuchten*, 1980; *Mualem*, 1976] define the soil hydraulic properties (equations 2 and 3), $\boldsymbol{s}$ could be composed of an array of effective soil hydraulic parameters $\{\alpha, n, \theta_{res}, \theta_{sat}, K_{sat}, \lambda\}$ for all soil i contained inside the pixel,

$$S_e = \frac{\theta(h) - \theta_{res}}{\theta_{sat} - \theta_{res}} = \left[\frac{1}{1 + |\alpha h|^n}\right]^m, \tag{2}$$

$$K(h) = K_{sat} S_e^{\lambda} \left[1 - \left(1 - S_e^{1/m}\right)^m\right]^2, \tag{3}$$

where S_e (–) is the relative saturation; K ($cm\ d^{-1}$) is the soil hydraulic conductivity; h is the pressure head (−cm); α (cm^{-1}) is defined as a shape parameter equivalent to the inverse of the bubbling pressure; n (–) is a shape parameter that accounts for the pore size distribution; θ_{res} ($cm^3\ cm^{-3}$) and θ_{sat} ($cm^3\ cm^{-3}$) are the residual and saturated soil moisture content, respectively; K_{sat} ($cm\ d^{-1}$) is the saturated hydraulic conductivity; and λ (–) is a shape parameter that accounts for tortuosity in the soil. *Van Genuchten* [1980] proposed m to be equal to $1 - 1/n$. An extended formulation using multiple vegetation-soil combinations (see Figure 1) is presented later in this paper.

[8] Linear mixture models (equation 1) have been used successfully in RS subpixel analyses [*Shimabukuro and Smith*, 1991; *Holben and Shimabukuro*, 1993; *Ferreira et al*., 2007] to produce area fractions of land use/land cover within a pixel in which their applications were generally confined at the spectral level of a RS image. Recent applications using temporal unmixing on state variables instead of spectral signatures have been shown to be promising [*Tateishi et al*., 2004; *Ines and Honda*, 2005].

2.2. Unmixing Algorithm

[9] We designed an unmixing method to solve $\boldsymbol{k}$ in equation (1) by employing a GA within a dynamic inverse simulation-optimization framework [*Ines and Honda*, 2005; *Ines et al*., 2006; *Ines and Mohanty*, 2008a, 2008b, 2008c, 2009]. For completeness, we describe the GA search process briefly. GAs are powerful search techniques combining the survival of the fittest mechanism with a structured yet randomized information exchange to search for solutions of complex search and optimization problems [*Holland*, 1975; *Goldberg*, 1989]. The search spaces of the unknown parameters (in this study, $\boldsymbol{s}_i$ and a_i) are discretized into finite lengths and then coded as sets of binary substrings (in binary GAs)

to form a string structure called a chromosome. The procedure starts by randomly generating a set of chromosomes (called a population) serving as starting search positions at the search surface. The chromosomes are individually evaluated (here, the simulation model is invoked using $\boldsymbol{s}_i$ and a_i) to determine their suitability based on a given fitness function. The chromosomes then go through the process of selection, crossover, and mutation. Based on their fitness, they compete to be selected, mate, and reproduce for the next generation. During selection, the fitter chromosomes survive and the weaker chromosomes die. The selected chromosomes then randomly mate to exchange genetic information through the process of crossover and produce offspring. The resulting new chromosomes are subjected to mutation to infuse fresh genetic materials for the new generation and to restore certain genetic characteristics that were lost due to degeneracy. The processes of selection, crossover, and mutation are repeated for many generations until the best possible solution is achieved. This solution is the fittest chromosome that evolved after many generations. We chose GAs to solve the mixed-pixel problem (equation (1)) over traditional optimization techniques [e.g., *Shimabukuro and Smith*, 1991], because they are easy to handle and implement, and they are proven to be very powerful for solving highly nonlinear, discontinuous combinatorial problems [*Goldberg*, 1989; *Ritzel et al*., 1994; *Cieniewski et al*., 1995; *Cai et al*., 2001; *Ines and Honda*, 2005; *Wang and Cai*, 2007]. Details of the GAs can be found in *Goldberg* [1989].

[10] We used a modified micro-GA as our search algorithm. This GA uses a micropopulation to explore the search surface. Its micropopulation restarts when most of the chromosomes are similar using a lesser degree of bit positioning-similarity criterion [*Krishnakumar*, 1989; *Carroll*, 1998; *Ines and Droogers*, 2002]. It applies a creep mutation operator to alter the chromosomes at the real space (base 10) and allows an intermittent jump mutation to occur with the binary chromosomes (base 2). Other details of the algorithm can be found elsewhere [e.g., *Ines and Honda*, 2005; *Ines and Mohanty*, 2008b, 2008c]. Micro-GA is suited well for this application because it improves computational efficiency, which is very important in coupled dynamic model (GA systems).

[11] The inverse model is composed of a dynamic field-scale simulation model SWAP [*Van Dam et al*., 1997; *Van Dam*, 2000] that simulates the SWAP interactions combined with the GA. SWAP is a well validated [*Wesseling and Kroes*, 1998; *Sarwar et al*., 2000; *Droogers et al*., 2000, *Ines and Droogers*, 2002; *Singh et al*., 2006a, 2006b], variably saturated flow model that solves the 1-D Richards equation to simulate the soil moisture dynamics in a vertical soil column using a robust implicit finite difference scheme [*Belmans et al*., 1983]. It uses the Mualem-Van Genuchten equations (equations (2) and (3)) [*Van Genuchten*, 1980; *Mualem*, 1976] to define the soil hydraulic properties. SWAP considers the time-dependent top boundary conditions in terms of either a flux or a given head, controlled dynamically based on a given set of nested criteria [*Van Dam et al*., 1997] related to the atmospheric forcings and hydrologic conditions at the soil surface. The bottom-boundary condition can be imposed in various forms (Dirichlet, Neumann, or Cauchy type). The SWAP model is an integrated water management tool containing irrigation and drainage modules as well as process-based crop growth models for simulating the impacts of weather, soil type, plant type, and water management practices on the growth and development of crops. Detailed descriptions of SWAP can be found in *Van Dam et al*. [1997] and *Van Dam* [2000].

[12] We designed the unmixing algorithm as follows. The observed (preferably, downscaled) RS near-surface soil moisture θ_t^{RS} in a pixel at any time t can be expressed by

$$\theta_t^{\mathrm{RS}} = \overline{\theta}_t(\boldsymbol{k}) + e_t, \quad \forall t. \tag{4}$$

The unmixing process can then be framed as an optimization problem where the objective is to minimize the total error $\Phi(\boldsymbol{k})$ (equation (5)) between the simulated and observed pixel-based near-surface soil moistures to find $\boldsymbol{k}$. The optimization problem is bounded by equations (6) and (7) and the allowable minimum and maximum values of the $\boldsymbol{s}_i$ components of $\boldsymbol{k}$ (equation (8))

$$\Phi(\boldsymbol{k}) = \mathrm{Min}\left\{\frac{1}{T}\sum_{t=1}^{T}|e_t|\right\} = \mathrm{Min}\left\{\frac{1}{T}\sum_{t=1}^{T}|\theta_t^{\mathrm{RS}} - \overline{\theta}_t(\boldsymbol{k})|\right\}, \tag{5}$$

subject to

$$\sum_{i=1}^{N} a_i = 1.0 \tag{6}$$

$$0 \le a_i \le 1.0, \qquad \forall i \tag{7}$$

$$\boldsymbol{s}_i^{\mathrm{Min}} \le \boldsymbol{s}_i \le \boldsymbol{s}_i^{\mathrm{Max}}, \qquad \forall i, \tag{8}$$

where $\overline{\theta}_t(\boldsymbol{k})$ ($\mathrm{cm}^3\ \mathrm{cm}^{-3}$) is the simulated resultant pixel-based soil moisture for given $\boldsymbol{k}$ at time t (see equation 1), θ_t^{RS} ($\mathrm{cm}^3\ \mathrm{cm}^{-3}$) is the corresponding observed RS near-surface soil moisture data, and T is the total number of time steps (days).

[13] The unmixing process works as follows: GA searches for $\boldsymbol{k}$, whereas SWAP uses the $\boldsymbol{s}$ component of $\boldsymbol{k}$ (recall that $\boldsymbol{k} = \{\boldsymbol{s}_{i=1,\ldots,N}, a_{i=1,\ldots,N}\}$) to simulate the representative (local) temporal near-surface soil moistures of all soil types contained within the pixel. The a_i components of $\boldsymbol{k}$ are applied to the corresponding θ_{it}, summed across all soil types to be compared with θ_t^{RS} for time t.

[14] The GA search is implemented using the following formalism. A penalized form of the objective function (equation (5)) using the modified penalty method of *Chan-Hilton and Culver* [2000] is formulated as follows:

$$Z(\boldsymbol{k}) = \mathrm{Min}\left\{\frac{1}{T}\sum_{t=1}^{T}|\theta_t^{\mathrm{RS}} - \overline{\theta}_t(\boldsymbol{k})| \times (1 + \mathrm{Penalty}\,(\boldsymbol{k}))\right\}, \tag{9}$$

where

$$\mathrm{Penalty}\,(\boldsymbol{k}) = \sum_{r=1}^{R}\delta_r\Theta_r, \tag{10}$$

and Θ_r is the set of constraints and δ_r is the corresponding penalty coefficient if the constraints are violated.

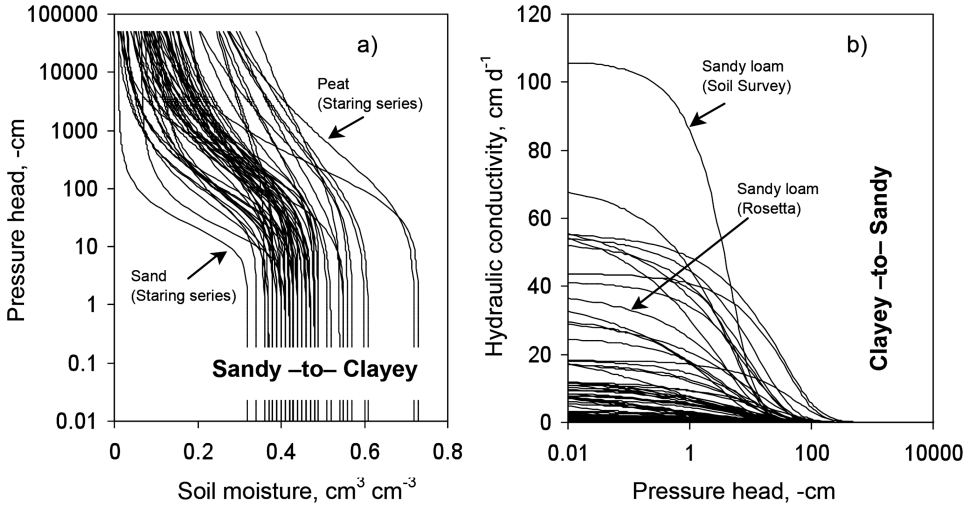

Figure 2. (a) Soil-water retention, $\theta(h)$, and (b) hydraulic conductivity, $K(h)$, curves of 64 soil data from different sources: HYPRES, Staring series, UNSODA, USDA-SCS (Soil Survey), and Rosetta.

[15] Since equations (7) and (8) are interval constraints, which can be directly coded in the GA as search spaces for $\boldsymbol{s}$ and a, only the equality constraint (equation (6)) was considered in equation (10) as shown below (hence $R = 1$, where r is the index for constraints):

$$\Theta_r = \left\{1 - \sum_{i=1}^{N} a_i\right\}^2 \quad (r = 1). \tag{11}$$

[16] If a chromosome (denoted by $\boldsymbol{p}$ ($\boldsymbol{p} \neq \boldsymbol{k}$)) violates the constraint of area fractions within the pixel the following rule is applied:

$$\text{if}\left(1 - \sum_{i=1}^{N} a_i \neq 0\right), \delta_r = 20; \text{otherwise}, \delta_r = 0 \; (r = 1). \tag{12}$$

Table 1. Area Fractions of Soil-Vegetation Combinations Used in the Numerical Experiments[a] (See Figure 1)

Soil-Vegetation	Area Fractions (a_{ij})[b]
(1) 1 Vegetation-3 Soils Combinations[c]	
Soils	
s_1	0.333 . . .
s_2	0.333 . . .
s_3	0.333 . . .
Total (s_1, s_2, s_3)	1.0
Vegetation	
v_1	1.0
Total (v_1)	1.0
s-v combinations	
s_1v_1	0.333 . . .
s_2v_1	0.333 . . .
s_3v_1	0.333 . . .
Total (s_1v_1, . . . , s_3v_1)	1.0
(2) 2 Vegetations-3 Soils Combinations (Depicted in Figure 1)	
Soils	
s_1	0.30556
s_2	0.34444
s_3	0.35
Total (s_1, s_2, s_3)	1.0
Vegetations	
v_1	0.5333
v_2	0.4667
Total (v_1, v_2)	1.0
s-v combinations	
s_1v_1	0.00556
s_2v_1	0.31667
s_3v_1	0.21111
s_1v_2	0.30
s_2v_2	0.02778
s_3v_2	0.13889
Total (s_1v_1, . . . , s_3v_2)	1.0

[a] s_1, sandy loam (ID = 1); s_2, silt loam (ID = 33); s_3, clay loam (ID = 40); v_1, wheat (*Triticum aestivum*); v_2, soybean (*Glycine max*). Soil IDs are derived from the lookup table of soil hydraulic properties (not shown).

[b] See section 2.2; i, index for soils; j, index for vegetations.

[c] Area fractions of soils under the simple case are slightly different from the complex case (Figure 1) to further test the robustness of the GA-based unmixing method. Area fraction of one means 100% of the pixel.

Table 2. Representations of the Unmixing Parameters in the GA

Unmixing Parameter	Search Space: Minimum Values	Search Space: Maximum Values	Number of Bits (L)	2^L
(1) 1 Vegetation-3 Soils Combinations				
s_1	1	64[a]	6	64
s_2	1	64	6	64
s_3	1	64	6	64
a_1	0	1.0	8	256
a_2	0	1.0	8	256
a_3[b]				
(2) 2 Vegetations-3 Soils Combinations				
s_1	1	64	6	64
s_2	1	64	6	64
s_3	1	64	6	64
a_{11} (s_1v_1)	0	1.0	8	256
a_{21} (s_2v_1)	0	1.0	8	256
a_{31} (s_3v_1)	0	1.0	8	256
a_{12} (s_1v_2)	0	1.0	8	256
a_{22} (s_2v_2)	0	1.0	8	256
a_{32}[c] (s_3v_2)				

[a] The total number of soil units considered in the lookup table of soil hydraulic properties.

[b] $a_N = 1 - \sum_{i=1}^{N-1} a_i$.

[c] $a_{NM} = 1 - \left(\sum_{j=1}^{M-1}\sum_{i=1}^{N} a_{ij} + \sum_{j=M}^{M}\sum_{i=1}^{N-1} a_{ij}\right)$.

Table 3. GA Parameters and SWAP Modeling Scenarios Used in the Unmixing Experiments[a]

	Numerical Experiments	Experiments Under Uncertainty (Numerical)	SMEX05 Field Experiments (Actual)	SGP97 Airborne-RS Footprint (Actual)
		GA Parameters		
Number of population	10, 20, 30	30	30	30
p_{creep}	0.1, 0.2, ..., 1.0	0.1, 0.2, ..., 1.0	0.1, 0.2, ..., 1.0	0.1, 0.2, ..., 1.0
p_{cross}	0.5	0.5	0.5	0.5
Seed	−1000	−1000	−1000	−1000
Intermittent p_{mutate}[b]	0.05	0.05	0.05	0.05
Number of generations	5000/search restart[d]	5000/search restart	5000/search restart	5000/search restart
Number of search restarts	8	8	8	5
		Modeling Conditions		
Top boundary conditions[c]	Time-dependent flux/head	Time-dependent flux/head	Time-dependent flux/head	Time-dependent flux/head
Bottom-boundary conditions	Free drainage (FD) $\frac{\partial H}{\partial z} = \frac{\partial (h+z)}{\partial z} = 1$	(1) FD	(1) FD	(1) FD
		(2) Variable groundwater table depths (GWL) (varied from 100, 150, 200 cm below soil surface)	(2) Variable groundwater table depths (GWL) (varied from 100, 150, 200, 250, 300, 390 cm below soil surface)	(2) Variable groundwater table depths (GWL) (varied from 100, 150, 200, cm below soil surface)
Initial conditions	$h(z,t=0) = -100$ cm; $0 \le z \le z_{max}$	(1) FD case: $h(z,t=0) = -100, -500, -1000$ cm; $0 \le z \le z_{max}$	(1) FD case: $h(z,t=0) = -100, -500, -1000$ cm; $0 \le z \le z_{max}$	(1) FD case: $h(z,t=0) = -100, -500, -1000$ cm; $0 \le z \le z_{max}$
		(2) GWL case: $h(z,t=0) \sim$ equilibrium with initial groundwater table depths; $0 \le z \le z_{max}$	(2) GWL case: $h(z,t=0) \sim$ equilibrium with initial groundwater table depths; $0 \le z \le z_{max}$	(2) GWL case: $h(z,t=0) \sim$ equilibrium with initial groundwater table depths; $0 \le z \le z_{max}$

[a] H, total hydraulic head (cm); h, pressure head (−cm); z, soil depth (cm; positive upward); t, time (days).
[b] Occurring at the 25th, 50th, 75th, and 85th percentiles of the maximum number of generations per search restart.
[c] Based on a given nested criteria [*Van Dam et al*., 1997] related to atmospheric forcings and hydrologic conditions at the soil surface.
[d] Search restart is different from micropopulation restarts (see section 2.2). In every search restart, the converging population of the 5000th generation is used as the initial population for the next new 5000 generations [see *Goldberg*, 2002].

The penalty coefficient (δ_r) value was chosen arbitrarily in this study; this can be chosen by sensitivity analysis. A too large value of δ_r will penalize heavy (hence killed) chromosomes with below average fitness but may contain genetic information that when shared with other chromosomes could trigger generation of the solution. The purpose is to promote diversity while exploiting good genetic traits among all individuals in the population.

[17] We defined the fitness function as follows:

$$\text{fitness}\,(\boldsymbol{p}) = \text{Max}\,[Z(\boldsymbol{k})]^{-1}, \tag{13}$$

which indicates that fitness ($\boldsymbol{p}$) is maximized if $Z(\boldsymbol{k})$ is minimized.

[18] The chromosome $\boldsymbol{p}$ was designed to reduce the dimensionality [*Michalewicz*, 1996] of the unmixing problem. Since $\sum_{i=1}^{N} a_i = 1$, we can express $a_N = 1 - \sum_{i=1}^{N-1} a_i$. We can then design $\boldsymbol{p} = \left\{\boldsymbol{s}_{i=1,\ldots,N}, a_{i=1,\ldots,N-1}\right\}$, thus reducing the number of unknown parameters (in $\boldsymbol{p}$), consequently $\boldsymbol{k} = \{\boldsymbol{p}, a_{i=N}\}$. The chromosome $\boldsymbol{p}$ was coded as a binary string structure in GA using the linear mapping technique (from base 2 to base 10) of *Goldberg* [1989].

[19] The unmixing problem described in equations (5)–(8) was extended into multiple soil-vegetation combinations (see Figure 1). The number of area fractions (i.e., the combinations of soils and vegetations) within the pixel would increase to $N \times M$, where N and M are the number of soil types and vegetation types, respectively, considered in the pixel. The simulated resultant pixel-based soil moisture $\overline{\theta}_t(\boldsymbol{k})$ for time t is extended as follows:

$$\overline{\theta}_t(\boldsymbol{k}) = \sum_{j=1}^{M}\sum_{i=1}^{N} a_{ij}\theta_{ijt} + e_t, \quad \forall t, \tag{14}$$

and $\boldsymbol{p} = \left\{\boldsymbol{s}_{i=1,\ldots,N}, a_{i=1,\ldots,N-1;j=1,\ldots,M-1}\right\}$. Therefore, $\boldsymbol{k} = \left\{\boldsymbol{p}, a_{i=N;j=M}\right\}$, where i and j are the indices for soil types and vegetation types, respectively. The remaining parts of the unmixing algorithm were adjusted to accommodate the extended unmixing problem.

[20] Analyzing the components of equation (14) can give us an idea to the contributions of vegetations and soils (Figure 1) into the resultant pixel-based soil moisture (shown in equation (15)):

$$\begin{aligned}
&(j=1; i=1,\ldots,N) && a_{1,1}(.) + a_{2,1}(.) + \ldots + a_{N-1,1}(.) + a_{N,1}(.) + e\\
&(j=2; i=1,\ldots,N) && a_{1,2}(.) + a_{2,2}(.) + \ldots + a_{N-1,2}(.) + a_{N,2}(.) + e\\
&\ldots && \ldots\\
&(j=M-1; i=1,\ldots,N) && a_{1,M-1}(.) + a_{2,M-1}(.) + \ldots + a_{N-1,M-1}(.) + a_{N,M-1}(.) + e\\
&(j=M; i=1,\ldots,N) && a_{1,M}(.) + a_{2,M}(.) + \ldots + a_{N-1,M}(.) + a_{N,M}(.) + e
\end{aligned} \tag{15}$$

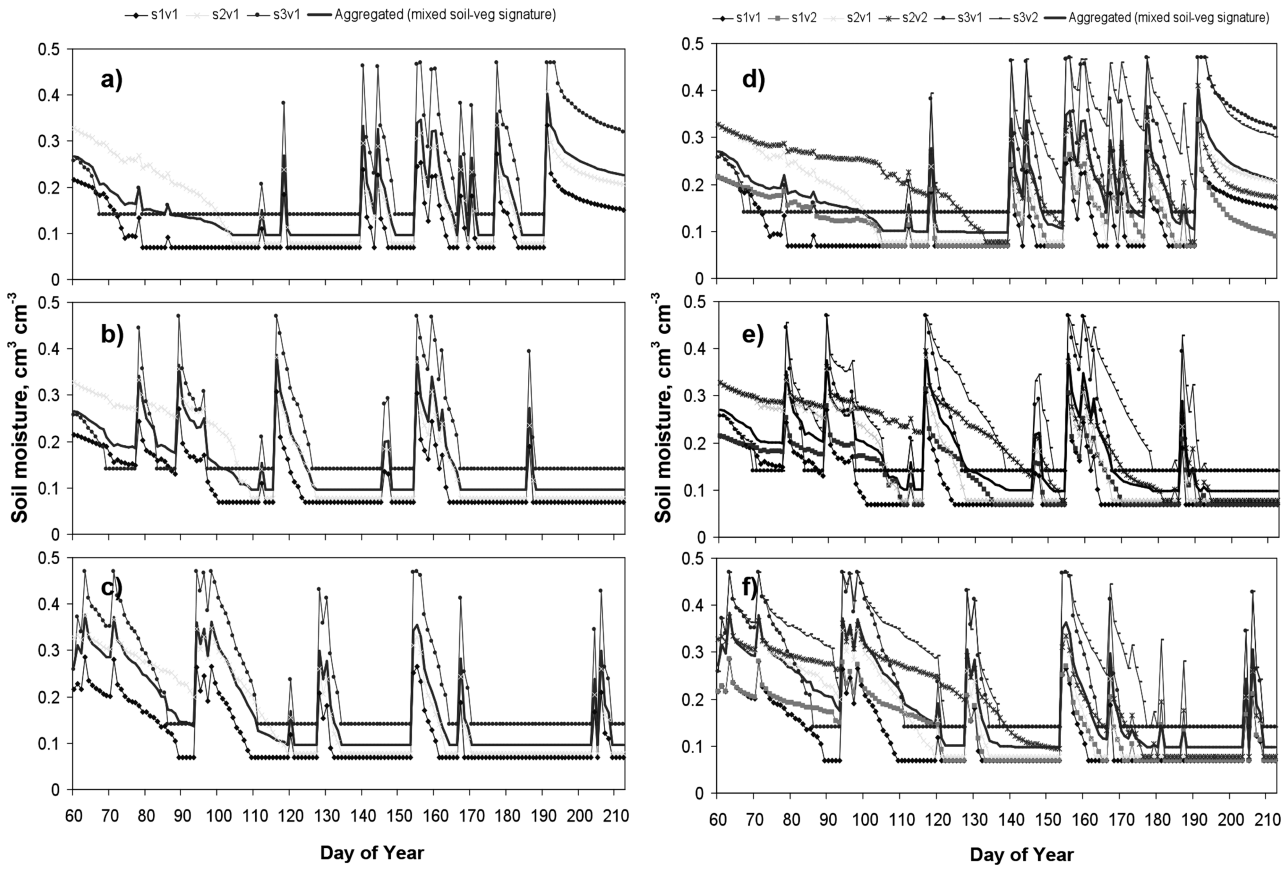

Figure 3. Synthetic soil moisture data used in the numerical experiments under (a–c) simple and (d–f) complex soil-vegetation combinations under (a, d) dry, (b, e) relatively wet, and (c, f) wet years. *Note*: s_1, sandy loam; s_2, silt loam; s_3, clay loam; v_1, wheat; v_2, sorghum.

where $(\cdot)$ denotes the θ_{ijt}. The row components (j=1, …, M) in equation 15 suggest the contributions of vegetation types to the resultant pixel-based soil moisture, whereas the column components (i = 1, …, N) suggest the contributions of soil types.

2.3. Soil Hydraulic Database: Lookup Table Approach

[21] Let us consider the one vegetation-three soils mixed-pixel problem (equations (5)–(8)) and define $\boldsymbol{s}_i$ in a traditional way, $\boldsymbol{s}$ could comprise 18 Mualem-Van Genuchten soil hydraulic parameters (i.e., $\{\alpha_i, n_i, \theta_{resi}, \theta_{sati}, K_{sati}, \lambda_i\}_{i=1,\ldots,3}$), this would lead to a very large combinatorial problem. To simplify $\boldsymbol{s}_i$ and to reduce dimensionality of the unmixing problem, we applied a lookup table method to represent an array of soil hydraulic properties of local-scale (homogenous) soil units. The lookup table was developed using existing soil hydraulic databases from the literature, namely, Unsaturated Soil Database (UNSODA) [*Leij et al.*, 1999], United States Department of Agriculture - Soil Conservation Service

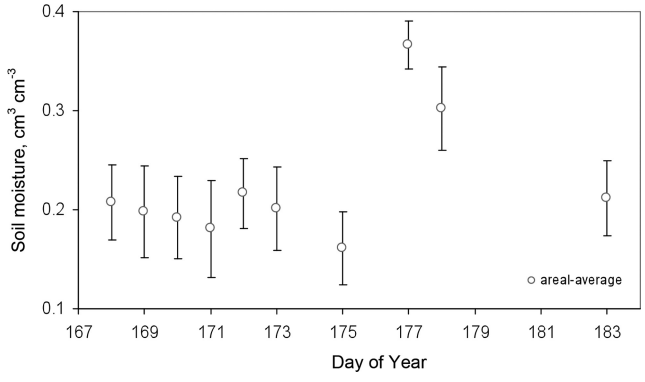

Figure 4. In situ near-surface (0–5 cm) soil moisture data in WC11 field during SMEX05 campaign. Error bars indicate one standard deviation.

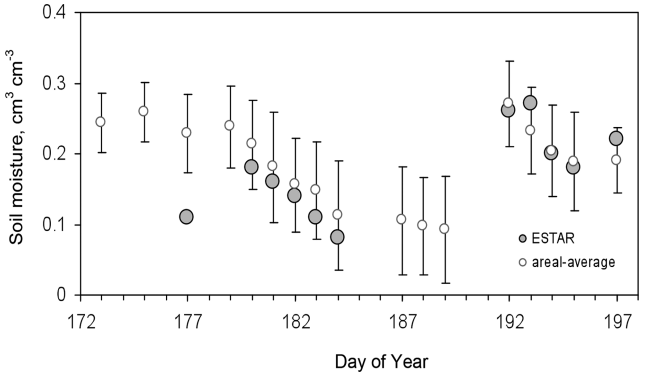

Figure 5. In situ and ESTAR near-surface (0–5 cm) soil moisture data in LW21 field during SGP97 campaign. Error bars indicate one standard deviation.

Table 4. Solutions of the Unmixing Problem Under *Simple Soil-Vegetation Case* (Three Soils-One Vegetation) in Idealized Modeling

Categories	Effective Soil Hydraulic Parameters						Average Area Fraction ($s_i v_1$)	Standard Deviation (SD) Area Fraction
	α	n	θ_{res}	θ_{sat}	K_{sat}	λ		
				Base Values				
s_1: sandy loam	0.021	1.61	0.067	0.37	41.6	0.5	0.333	
s_2: silt loam	0.012	1.39	0.061	0.43	30.5	0.5	0.333	
s_3: clay loam	0.030	1.37	0.129	0.47	1.8	0.5	0.333	
				(a) Dry Year				
s_1	0.021	1.61	0.067	0.37	41.6	0.5	0.332	0.004
s_2	0.012	1.39	0.061	0.43	30.5	0.5	0.333	0.005
s_3	0.030	1.37	0.129	0.47	1.8	0.5	0.334	0.006
				(b) Relatively Wet Year				
s_1	0.021	1.61	0.067	0.37	41.6	0.5	0.331	0.003
s_2	0.012	1.39	0.061	0.43	30.5	0.5	0.333	0.001
s_3	0.030	1.37	0.129	0.47	1.8	0.5	0.337	0.003
				(c) Wet Year				
s_1	0.021	1.61	0.067	0.37	41.6	0.5	0.330	0.021
s_2	0.012	1.39	0.061	0.43	30.5	0.5	0.333	0.011
s_3	0.030	1.37	0.129	0.47	1.8	0.5	0.337	0.012

(USDA-SCS) (Soil Survey) [*Carsel and Parrish*, 1988], Hydraulic Properties of European Soils (HYPRES) [*Wösten et al*., 1999], Staring soil database [*Wösten et al*., 1994], and Rosetta [*Schaap et al*., 1999], whose soil-water retention $\theta(h)$ and hydraulic conductivity $K(h)$ curves are depicted in Figure 2; each of the soils represented by the soil hydraulic curves [$\theta(h)$, $K(h)$] is assigned an ID (identification number). By using a lookup table, we can redesign $\boldsymbol{s}_i$ to consist only of three unknown parameters, corresponding to the unit ID of the three soils from the lookup table of soil hydraulic properties; this process is called regularization.

2.4. Case Studies

[22] We tested the unmixing method using idealized experiments that include simple and complex mixed pixels. Idealized experiments include running the SWAP model in forward mode for known soils, vegetations, management (these case studies are rainfed), initial/boundary conditions, and climate forcings in the synthetic pixel and then aggregating the simulated near-surface soil moistures based on the known area fractions of soils-vegetations in the pixel, and then use it to inversely estimate the original subgrid pixel properties. Afterward, we validated the method using actual soil moisture data from a field and an airborne-RS footprint if it works under real-world conditions. Weather data required by SWAP include daily rainfall, maximum and minimum temperature, solar radiation, humidity, and wind.

[23] Table 1 shows the area fractions of soils and vegetations, contained within the modeling domains, used for the simple and complex soil-vegetation cases. The unmixing method aims to calculate back those area fractions using information from soil moisture time series. Table 2 also

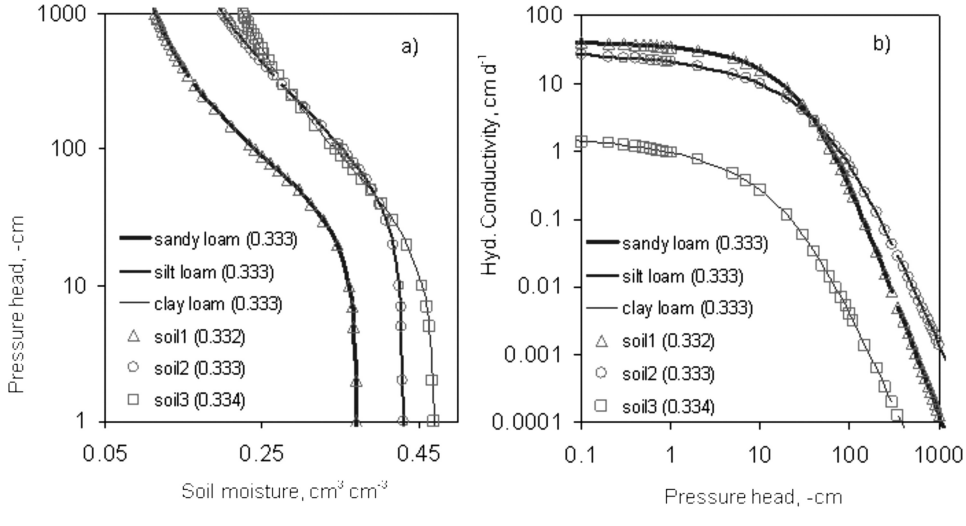

Figure 6. Sample results of unmixed (a) soil-water retention curve, $\theta(h)$, and (b) hydraulic conductivity curve, $K(h)$ in idealized modeling under simple soil-vegetation case (three soils-one vegetation) during dry year. *Notes*: sandy loam, silt loam, and clay loam are the reference soils; soil1, soil2, and soil3 are the corresponding solutions, respectively. Area fractions are given in parentheses.

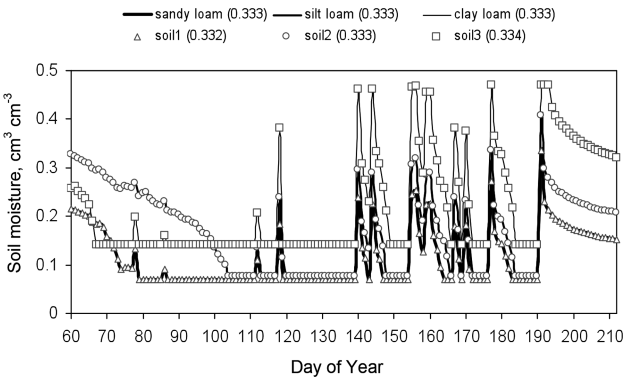

Figure 7. Sample results of unmixed soil moisture in idealized modeling under simple soil-vegetation case (three soils-one vegetation) during dry year. *Notes*: sandy loam, silt loam, and clay loam are the reference soils; soil1, soil2, and soil3 are the corresponding solutions, respectively. Area fractions are given in parentheses.

shows how the unmixing parameters were represented in GA. These are the range of search spaces used for each unmixing parameters, and the length of strings used to represent the value of each parameter. For simple soil-vegetation scenario (three soils and one vegetation), six unmixing parameters were determined but only five of them were coded in the GA, since $\sum_{i=1}^{N} a_i = 1$; hence, one area fraction can be expressed as a residual of the expression above (section 2.2). Similarly, with complex soil-vegetation scenario (three soils and two vegetations), nine unmixing parameters were determined, but only eight (i.e., components of $\boldsymbol{p}$) of these parameters were coded as binary substrings in GA. Table 3 summarizes the GA parameters used in the unmixing method runs and SWAP initial and boundary conditions used during those runs under the idealized and actual validation experiments.

2.4.1. Idealized Numerical Experiments

2.4.1.1. Simple Soil-Vegetation Combination (One Vegetation-Three Soils)

[24] The simple case includes a modeling domain containing one vegetation-three soils combination, and the complex one includes a two vegetations-three soils combination (see Figure 1). Figures 3a–3c show the simulated representative (local-scale) near-surface soil moistures used in the unmixing of the one vegetation-three soils combination problem. These representative near-surface soil moisture data were simulated within a modeling domain containing three soil textures (sandy loam, silt loam, and clay loam) with one vegetation cover (wheat) for the whole domain during a cropping season (March–July) in a dry, relatively wet, and wet year (classification based on Northern Texas climate) under nonirrigated conditions. The vertical soil column was assumed to be 2 m depth; other conditions used in the simulations are given in Table 3. Details of the simulations can be found in *Ines and Mohanty* [2008a, 2008b].

[25] The lookup table search implementation for soil hydraulic properties (representing $\boldsymbol{s}_i$) allowed the development of a GA dynamic-static chromosome evaluation to generate a data cube that serves as a meta-model for the inverse problem. The usual approach used for evaluating chromosomes in coupled methodologies like SWAP-GA is by a dynamic model linkage where the proposed chromosome $\boldsymbol{p}$ is directly transferred to SWAP for simulating the modeled physical system responses. This dynamic interaction between model and the search algorithm is often costly (in terms of computational time) for population-based search methods like GA, unless designed under a parallel infrastructure [*Ines and Honda*, 2005]. The proposed hybrid-chromosome evaluation is envisaged to save computational time in solving the unmixing problem without sacrificing accuracy of results. The mechanics of the hybrid-dynamic-static chromosome evaluation are described below.

[26] A 3-D table (data cube) of soil-vegetation response (i.e., near-surface soil moisture) was developed to store modeled system responses to a particular $s_i v_j$ combination, given the climatic and environmental forcings and boundary conditions. The soil-vegetation-response data cube is filled dynamically with simulated near-surface soil moisture data, as SWAP simulates an *s-v* combination (see Table 1). Until data space in the data cube is available for an *s-v* combination, SWAP is used to simulate specific *s-v* combination to evaluate $\boldsymbol{p}$. Otherwise, GA will use the data cube to get the modeled response for $\boldsymbol{p}$. The data cube comprises rows, containing time elements of soil moisture, and columns, containing the soil elements (soil ID) and, at the transverse direction, the vegetation elements.

[27] Together with the built-in time-saving scheme in the modified micro-GA [*Ines and Honda*, 2005; *Ines and Mohanty*, 2008b], the dynamic-static chromosome evaluation made the search process more efficient, allowing us to explore better the unmixing problem by considering more scenarios in the experiments (see Table 3).

2.4.1.2. Complex Soil-Vegetation Combination (Two Vegetations-Three Soils)

[28] Two vegetations (wheat and soybean) were used for the complex soil-vegetation scenario (Figure 1). The representative soil moisture data for each s-v combination in the complex scenario (see Table 1) are shown in Figures 3d–3f in which the mixed soil moisture was used to estimate the components of extended $\boldsymbol{k}$ variable (see section 2.2).

Table 5. Performance of the Unmixing Solutions Under Simple and Complex Soil-Vegetation Cases in Idealized Modeling[a]

Categories	Statistics	
	R	RMSE
(1) Simple Soil-Vegetation Case (3 Soils-1 Vegetation)		
(a) Dry year		
$\boldsymbol{s}_{i=1,\ldots,3}$,$v_1$	0.999	8.69E−05
(b) Relatively wet year		
$\boldsymbol{s}_{i=1,\ldots,3}$,$v_1$	0.999	4.65E−04
(c) Wet year		
$\boldsymbol{s}_{i=1,\ldots,3}$,$v_1$	0.999	2.07E−04
(2) Complex Soil-Vegetation Case (3 Soils-2 Vegetations)		
(a) Dry year		
$\boldsymbol{s}_{i=1,\ldots,3}$,$v_1$,$v_2$	0.999	5.48E−04
(b) Relatively wet year		
$\boldsymbol{s}_{i=1,\ldots,3}$,$v_1$,$v_2$	0.999	5.13E−04
(c) Wet year		
$\boldsymbol{s}_{i=1,\ldots,3}$,$v_1$,$v_2$	0.999	2.64E−04

[a] v_1, wheat; v_2, soybean. Individual $s_i v_j$ performance is not shown as their *R* and RMSE values are approximately 1.0 and approximately 0.0, respectively.

Table 6. Solutions of the Unmixing Problem Under *Complex Soil-Vegetation Case* in Idealized Modeling (Three Soils-Two Vegetations)

	Effective Soil Hydraulic Parameters						Vegetation 1, v_1 (Wheat)		Vegetation 2, v_2 (Soybean)	
Categories	α	n	θ_{res}	θ_{sat}	K_{sat}	λ	Average Area Fraction ($s_i v_1$)	SD Area Fraction	Average Area Fraction ($s_i v_2$)	SD Area Fraction
					Base Values					
s_1: sandy loam	0.021	1.61	0.067	0.37	41.6	0.5	0.006		0.30	
s_2: silt loam	0.012	1.39	0.061	0.43	30.5	0.5	0.32		0.03	
s_3: clay loam	0.030	1.37	0.129	0.47	1.8	0.5	0.21		0.14	
					(a) Dry Year					
s_1	0.021	1.61	0.067	0.37	41.6	0.5	0.012	0.010	0.280	0.014
s_2	0.012	1.39	0.061	0.43	30.5	0.5	0.325	0.009	0.032	0.005
s_3	0.030	1.37	0.129	0.47	1.8	0.5	0.204	0.016	0.148	0.011
					(b) Relatively Wet Year					
s_1	0.021	1.61	0.067	0.37	41.6	0.5	0.003	0.002	0.284	0.002
s_2	0.012	1.39	0.061	0.43	30.5	0.5	0.329	0	0.027	0
s_3	0.030	1.37	0.129	0.47	1.8	0.5	0.217	0.005	0.140	0.002
					(c) Wet Year					
s_1	0.021	1.61	0.067	0.37	41.6	0.5	0.004	0	0.294	0
s_2	0.012	1.39	0.061	0.43	30.5	0.5	0.318	0	0.027	0
s_3	0.030	1.37	0.129	0.47	1.8	0.5	0.216	0	0.141	0

2.4.1.3. Unmixing Under Uncertainty

[29] Data and modeling errors are inevitable in the real world. For this reason, we tested the GA-based unmixing method under uncertainty conditions. To account for data errors in the mixed soil moisture, we perturbed the "error-free" area-weighted soil moisture data from the idealized numerical experiment (only wet year scenario) applying $\theta' = \theta \times (1 + \boldsymbol{x}\xi)$; $\boldsymbol{x} \sim N(0,1)$; $-1 \leq \boldsymbol{x} \leq 1$, where θ' and θ are perturbed and "error-free" soil moistures, respectively; $\boldsymbol{x}$ is a normal random deviate with mean and standard deviation equal to 0 and 1, respectively; ξ is the error term. An error (ξ) of 30% was applied across the time series of noise-free mixed soil moisture. Ten perturbed soil moisture series were generated. The error term in the perturbation equation could be associated with measurement errors incurred during field data collection.

[30] To account for modeling errors, we consider that the initial and bottom-boundary conditions are both uncertain (Table 3). The top boundary condition was considered as time-dependent flux/head based on prevailing hydroclimatic conditions at the surface [see *Van Dam et al.*, 1997]. The bottom-boundary conditions were either considered as free draining (i.e., $\partial(h + z)/\partial z = 1$; thus, $q_{bot} = -K(h)$, where z is the depth, q_{bot} is the bottom flux) or governed by water table dynamics [*Van Dam et al.*, 1997]. Under a free-drainage condition, the soil profile was initialized using three different initial conditions at $h(z_{min} \leq z \leq z_{max}, t = 0) = -100, -500$, and -1000 cm. When water table depths were used as bottom boundaries, initial conditions were calculated in equilibrium with initial water table depths and were varied from 100, 150, and 200 cm from the soil surface.

[31] All 10 perturbed mixed soil moisture time series were used for solving the unmixing variable $\boldsymbol{k}$ (see section 2.2). For each perturbed-time series, SWAP is subjected to combinations of initial and boundary conditions to account for both data and modeling errors in the unmixing

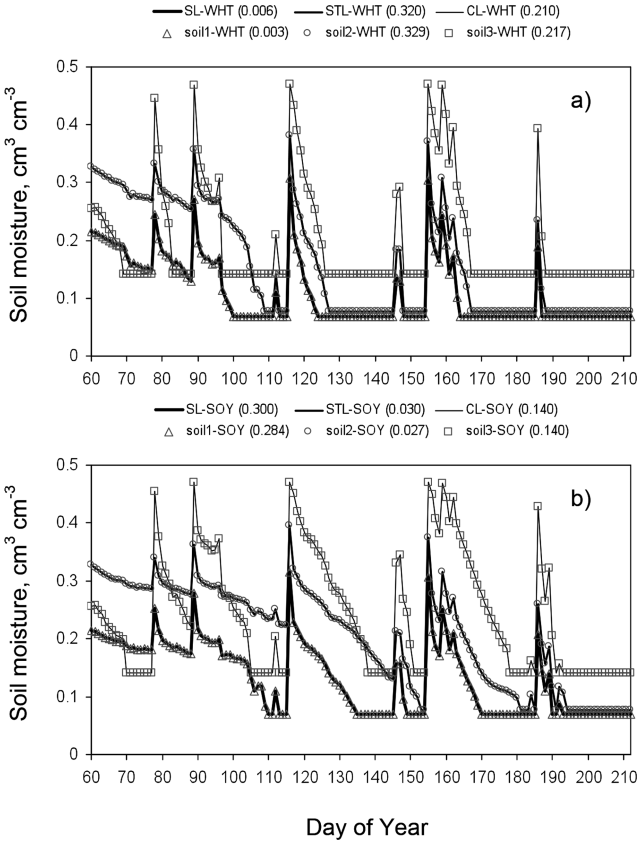

Figure 8. Sample results of (a) wheat and (b) soybean unmixed soil moisture in idealized modeling under complex soil-vegetation case (three soils-two vegetations) during relatively wet year. *Notes*: SL-WHT, sandy loam-wheat; STL-WHT, silt loam-wheat; CL-WHT, clay loam-wheat; SL-SOY, sandy loam-soybean; STL-SOY, silt loam-soybean; CL-SOY, clay loam-soybean; soil#-WHT, corresponding solutions under wheat crops; soil#-SOY, corresponding solutions under soybean crops (see equation (15)); Area fractions are given in parentheses.

Table 7. Solutions of the Unmixing Problem *Under Uncertainty in Simple Soil-Vegetation Case* in Idealized Modeling During *Wet Year* (Three Soils-One Vegetation)[a]

Categories	Effective Soil Hydraulic Parameters						Average Area Fraction ($s_i v_1$)	SD Area Fraction
	α	n	θ_{res}	θ_{sat}	K_{sat}	λ		
Base Values (FD Bottom Boundary; Initial Condition $h(z,t=0) = -100$ cm)								
s_1: sandy loam	0.021	1.61	0.067	0.37	41.6	0.5	0.333	
s_2: silt loam	0.012	1.39	0.061	0.43	30.5	0.5	0.333	
s_3: clay loam	0.030	1.37	0.129	0.47	1.8	0.5	0.333	
(a) FD Bottom-Boundary Conditions								
Initial condition $h(z, t = 0) = -100$ cm								
s_1	0.022	1.60	0.066	0.37	40.1	0.49	0.316	0.063
s_2	0.016	1.39	0.064	0.42	25.2	0.12	0.372	0.087
s_3	0.029	1.36	0.123	0.47	2.3	0.54	0.312	0.056
Initial condition $h(z, t = 0) = -500$ cm								
s_1	0.007	1.68	0.050	0.49	43.8	0.62	0.489	0.011
s_2	0.010	1.23	0.072	0.43	2.0	0.35	0.158	0.163
s_3	0.011	1.22	0.079	0.43	3.1	0.29	0.353	0.163
(b) Variable Groundwater Conditions								
GWL $= -100$ cm; initial condition $h(z,t=0)$: equilibrium with initial GWL								
s_1	0.039	1.54	0.053	0.40	45.6	0.84	0.504	0.191
s_2	0.021	1.37	0.067	0.42	17.6	0.43	0.165	0.162
s_3	0.017	1.29	0.110	0.44	5.8	0.33	0.332	0.170
GWL $= -150$ cm; initial condition $h(z,t=0)$: equilibrium with initial GWL								
s_1	0.033	1.38	0.047	0.42	47.6	0.86	0.438	0.033
s_2	0.028	1.40	0.080	0.44	30.0	0.37	0.407	0.053
s_3	0.011	1.16	0.078	0.40	4.6	0.44	0.155	0.057
GWL $= -200$ cm; initial condition $h(z,t=0)$: equilibrium with initial GWL								
s_1	0.028	1.49	0.041	0.38	44.6	0.27	0.369	0.118
s_2	0.022	1.31	0.061	0.44	29.1	0.50	0.269	0.132
s_3	0.022	1.25	0.090	0.43	7.9	−0.29	0.362	0.124

[a]Cases (a) and (b) are subjected with 30% data error.

experiments. The solutions from all the unmixing runs were analyzed to get the final results (i.e., soil and vegetation area fractions).

2.4.2. Field Experiments and Validation

2.4.2.1. Field Scale

[32] We also conducted unmixing experiments using actual in situ soil moisture data collected from WC11 field within the WC watershed, Iowa, during SMEX05 campaign [see *Ines and Mohanty*, 2008a, Figure 5]. According to Soil Survey Geographic Database (SSURGO) (http://soildatamart.nrcs.usda.gov), the soils in WC11 field boundary comprise loam, silt loam, and clay loam. Maize is the dominant crop. Soil moisture was measured from 62 locations using hand-held theta probes from 17 June to 2 July 2005. Because of weather related conditions, no data were collected on 23, 25, 28–30 June, resulting to 10 near-surface (0–5 cm) soil moisture data (62 sampling points across the field) available for WC11 field (Figure 4). Longer time series of soil moisture (hence, information) is, however, desired to capture the full range of soil moisture dynamics.

[33] In situ soil moisture data were mixed by arithmetic averaging to produce field-scale average soil moisture time series (see Figure 4). In the soil moisture unmixing experiments, we set three soils encompassing WC11 field based on a priori information from SSURGO. All simulations (Table 3) were done from January to December 2005, and only the simulated mixed soil moisture data coinciding with the SMEX05 campaign period (17 June to 2 July) were compared with the observations during unmixing. Simulations made prior to June 2005 were used for model spinning. The field was under corn cover during SMEX05 campaign. Daily weather data including rainfall, minimum and maximum temperature, wind speed, humidity, and solar radiation were collected from a nearby Soil Climate Analysis Network (SCAN) site at Ames, Iowa (http://www.wcc.nrcs.usda.gov/scan/).

2.4.2.2. Airborne-RS Scale

[34] We also conducted unmixing experiments (Table 3) at the scale of airborne-RS Electronically Scanning Thin Array Radiometer (ESTAR) at a selected grid (LW21) in LW watershed in Oklahoma during SGP97 [see *Ines and Mohanty*, 2009, Figure 2]. ESTAR pixel-based (800 m × 800 m) soil moisture products [*Jackson et al.*, 1995, 1999] at the LW21 site were extracted and used for the inverse modeling. In situ soil moisture (0–5 cm) across the field (49 sampling points) were measured from 18 June to 18 July 1997 [*Mohanty et al.*, 2002] and used for validation (Figure 5). The LW21 site is composed of silt loam, sandy loam, and loam soils according to SSURGO and covered by winter wheat (during SGP97 campaign) and short native grass. The growing period was set in SWAP model as 1 March to 27 June, although simulations were started 1 January for model spinning. Only those dates when ESTAR data are available were extracted and used in the inverse modeling. Daily weather data used in modeling were collected from the USDA-Agricultural Research Service micronet weather station (ARS 149) in Oklahoma.

2.5. Analysis of Results

[35] A filter was used to extract the most probable solutions from the converged GA populations. The filter was

Table 8. Performance of the Unmixing Solutions *Under Uncertainty in Simple Soil-Vegetation Case* in Idealized Modeling During *Wet Year* (Three Soils-One Vegetation)[a]

Categories	Statistics	
	R	RMSE
(a) FD Bottom-Boundary Conditions		
Initial condition $h(z,t=0) = -100$ cm		
s_1,v_1	0.985	0.028
s_2,v_1	0.998	0.014
s_3,v_1	0.970	0.028
$\boldsymbol{s}_{i=1,\ldots,3},v_1$	0.998	0.007
Initial condition $h(z,t=0) = -500$ cm		
s_1,v_1	0.925	0.035
s_2,v_1	0.910	0.074
s_3,v_1	0.975	0.030
$\boldsymbol{s}_{i=1,\ldots,3},v_1$	0.996	0.010
(b) Variable Groundwater Conditions		
GWL = −100 cm; initial condition $h(z,t=0)$: equilibrium with initial GWL		
s_1,v_1	0.994	0.021
s_2,v_1	0.970	0.047
s_3,v_1	0.998	0.010
$\boldsymbol{s}_{i=1,\ldots,3},v_1$	0.996	0.010
GWL = −150 cm; initial condition $h(z,t=0)$: equilibrium with initial GWL		
s_1,v_1	0.975	0.023
s_2,v_1	0.969	0.032
s_3,v_1	0.975	0.041
$\boldsymbol{s}_{i=1,\ldots,3},v_1$	0.998	0.008
GWL = −200 cm; initial condition $h(z,t=0)$: equilibrium with initial GWL		
s_1,v_1	0.985	0.035
s_2,v_1	0.975	0.041
s_3,v_1	0.991	0.023
$\boldsymbol{s}_{i=1,\ldots,3},v_1$	0.997	0.009

[a]Cases (a) and (b) are subjected with 30% data error.

implemented by log-transforming the fitness of the final populations (collected from all cases of varying population sizes, p_{creep} mutations, and number of generation restarts under an experiment, see Table 3); then those chromosomes whose log-fitness are above a threshold are extracted. Under the idealized numerical experiments, we used the top 1% (99% filter) as representative solutions to the inverse problem. Under uncertainty scenarios, we considered the top 5% (95% filter) as best possible solutions. For the actual field experiments, we applied a less strict filter [$>(\mu + 1\sigma)$], since there were significant uncertainties involved in the simulations. Correlation (R) and error analyses (root-mean-square error (RMSE)) were also used to evaluate the performance of the solutions.

3. Results and Discussion

3.1. Idealized Experiments

3.1.1. Simple Vegetation-Soil Combination

[36] This case exemplifies a pixel under full coverage by single vegetation, with three soils bounded by the pixel boundary. Under known modeling conditions, we run SWAP in forward mode for the one vegetation-three soils combinations to develop a time series of mixed near-surface soil moisture (Table 1), which were then used to unmix back the soils, and soil-vegetation fractions of the said pixel applying the unmixing algorithm presented here. To verify the robustness of the method, the experiments were replicated under a dry, relatively wet, and wet year. The vegetation cover for this synthetic experiment is wheat. The reference soils are sandy loam (s_1), silt loam (s_2), and clay loam (s_3), designated as soil IDs 1, 33, and 40 from the lookup table (not shown), whose corresponding Mualem-Van Genuchten soil hydraulic parameters are also contained in the lookup table. The objective is to estimate back these soil properties and their combinations within the study pixel based on the time series of mixed near-surface soil moisture.

[37] Table 1 shows the exact solutions for area fractions of the one vegetation-three soils unmixing problem, $s_1v_1 = s_2v_1 = s_3v_1 = 0.333$. The ability of the method to unmix the near-surface soil moisture and infer information about the soils in the pixel under this idealized case is shown in Table 4. For all replications, it can be seen that the soil signatures were exactly determined. This indicates that the unmixing algorithm was able to determine the soils whose soil hydraulic properties behave exactly as the soils bounded by the pixel contributing to the mixed near-surface soil moisture. In terms of eliciting the area fractions of soils bounded by the pixel, it can be seen that, on average, the unmixing algorithm was able to approximate the area fractions of soils associated with s_1, s_2, and s_3. It is interesting to note that under dry and relatively wet years, the determination of soil area fractions are more consistent (lower standard deviations) than during the wet year. Area fraction determination is critical, because it dictates the weight of a pure (i.e., downscaled) soil moisture time series to the overall pixel-based soil moisture.

[38] Figure 6 shows sample unmixed $\theta(h)$ and $K(h)$ solutions of the idealized one vegetation-three soils combination problem during the dry year. Since the derived sets of soil hydraulic properties behave exactly as the reference soils in the pixel, the downscaled $\theta(h)$ and $K(h)$ curves look exactly as the reference ones. Consequently, the downscaled soil moisture data behave exactly as the reference data (Figure 7) and, hence, the mixed soil moisture (Table 5). However, due to some variations in soil area-fraction determination in wet scenario (Table 4), some minor discrepancies between the reference and predicted mixed soil moisture are observed (Table 5).

3.1.2. Complex *V*egetation-*S*oil *C*ombination

[39] In most cases, there would be mixture of vegetations in a large RS pixel. This case tests the suitability of the unmixing algorithm to determine the area fractions of soil-vegetation combinations and their respective soil hydraulic properties and soil moisture dynamics, from a two vegetations-three soils mixing problem perspective. Again, under known climatic and environmental conditions (Table 3), we run SWAP in forward mode considering three soils: sandy loam, silt loam, and clay loam, with wheat and soybean vegetations. To develop the pixel-based soil moisture, the area fractions from Table 1 were applied to the individual s_iv_j soil moisture and then mixed. The unmixing algorithm was then applied to downscale mixed near-surface soil moisture to various soil-vegetation combinations. The experiment was also replicated using a dry, relatively wet, and wet year scenario.

[40] Table 6 shows the solutions of the unmixing problem under the complex soil-vegetation (3 × 2) combination

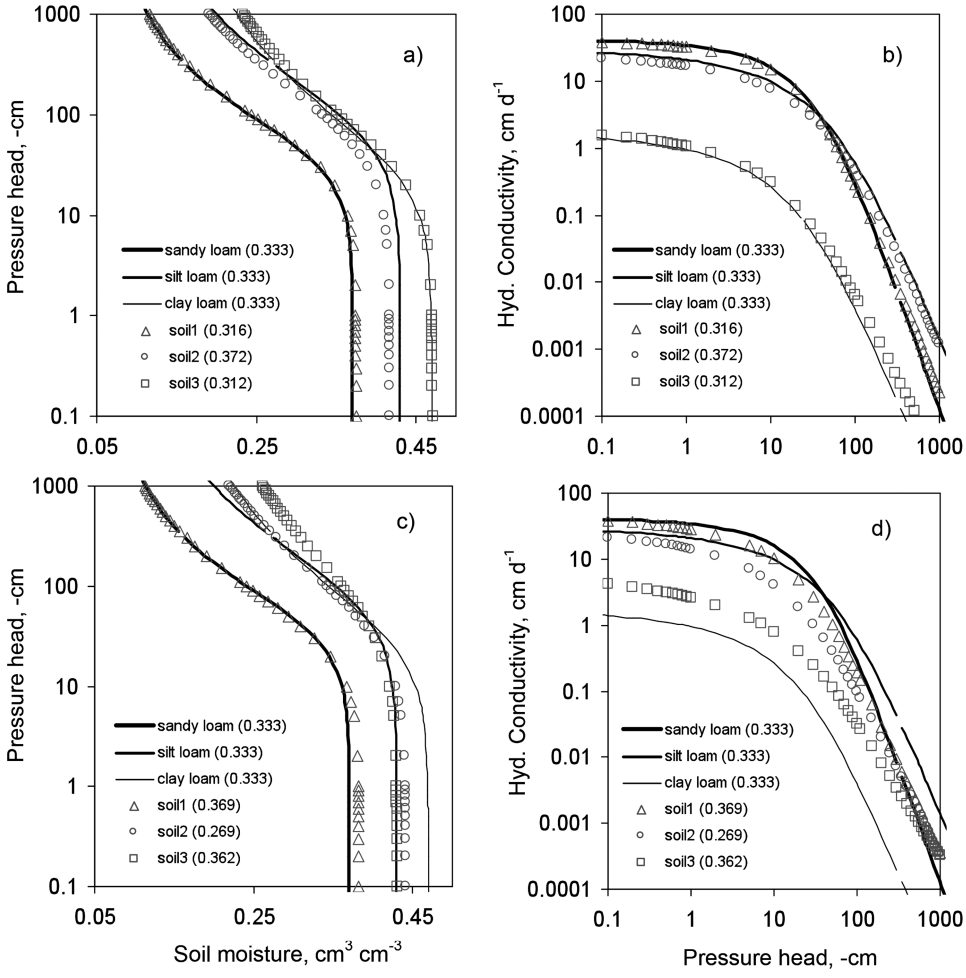

Figure 9. Sample results of unmixed soil-water retention curve, $\theta(h)$, and hydraulic conductivity curve, $K(h)$, in idealized modeling under uncertainty in simple soil-vegetation case (three soils-one vegetation) during wet year, (a, b) with only data error (30%) as source of uncertainty and (c, d) with both modeling error (groundwater bottom-boundary condition; GWL $= -200$ cm; initial condition $h(z,t=0)$: equilibrium with initial GWL) and data error (30%) as sources of uncertainty. *Notes*: sandy loam, silt loam, and clay loam are the reference soils; soil1, soil2, and soil3 are the corresponding solutions, respectively. Area fractions are given in parentheses.

for all replications. It can be seen that under this relatively complex scenario, the unmixing algorithm performed well in determining the complex combinations of soil hydraulic properties and their area fractions with vegetations encompassed in the pixel. Note however that the area fractions were not exactly determined but, on average, they are very near the vicinity of the exact solution (*base values*, Table 6). Some variations in the area fractions are also noticed in the solutions. The wet year scenario area fractions did not have variations, because the analysis filter only determined 3 (similar) solutions out of 40,000 generations from several experimentations (Table 3). Interesting to note is the ability of the unmixing algorithm to discern the smallest area fractions (s_1v_1) out from the pixel-based soil moisture signature, suggesting the possibility of applying the method in a generic way (i.e., n is the number of soils, and m is the number of vegetations, where $n, m > 2$) if no a priori ground information is available. The unmixing algorithm could possibly determine the appropriate number of soils and vegetations in a pixel by nullifying (area fractions ≈ 0) those that are not represented from the pixel-based soil moisture signature. Figure 8 shows how closely matched are the unmixed soil moisture time series and the reference data under the complex soil-vegetation combination in relatively wet year scenario. Because the solutions are very near to the base values (Table 6), the correlations and RMSE between predicted and reference soil moisture were exceptional even at the mixed level regardless of the discrepancies in the estimated area fractions (Table 5).

3.1.3. Soil Moisture Unmixing Under Uncertainty

[41] The experiments described above assume that modeling conditions and data are free from errors. In reality that is not the case, but the results above have provided useful insights about the ability of the unmixing algorithm to infer soil hydraulic properties, soil-vegetation fractions in a pixel, and in turn for downscaling soil moisture from a pixel-based soil moisture signature. The purpose of this section is to check if the exact/near-exact solutions can be

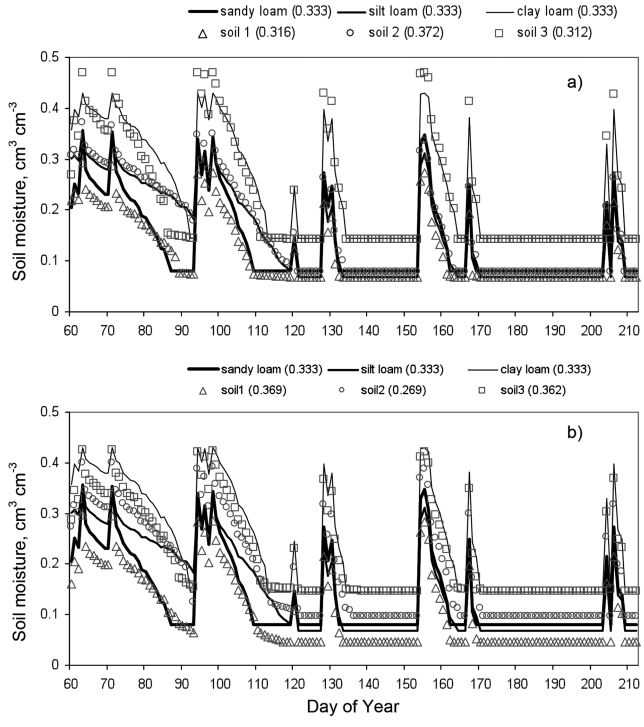

Figure 10. Sample results of unmixed soil moisture in idealized modeling *under uncertainty in soil-vegetation case* (three soils-one vegetation) during *wet year*, (a) with only data error (30%) as source of uncertainty and (b) with both modeling error (groundwater bottom-boundary condition; GWL = −200 cm; initial condition $h(z,t=0)$: equilibrium with initial GWL) and data error (30%) as sources of uncertainty. *Notes*: sandy loam, silt loam, and clay loam are the reference soils; soil1, soil2, and soil3 are the corresponding solutions, respectively. Area fractions are given in parentheses.

still derived if the unmixing problem was set up with data errors and modeling uncertainties. Here, we considered only the wet year case.

[42] Table 7 shows the solutions of the unmixing problem under uncertainty. When the only source of error is from the data (a 30% error was applied, see section 2.4.1.3), the area fractions of soils were still estimated reasonably well, and the soil hydraulic parameters are also reasonably close to the base values (see (a) free-drainage bottom-boundary conditions: initial condition $h(z,t=0) = -100$ cm]. This suggests that as long as the initial and boundary conditions are represented well, there is a high possibility that near-optimal solutions can be achieved if the error in the data source is at low-to-moderate level. However, as the sources of errors are compounded by data and boundary/initial conditions, the area-fraction determination and soil hydraulic parameter estimations were less than ideal. If we consider the overall performance of these solutions, the correlations and RMSE of the individual soil moisture series $s_i v_j$ with respect to the reference values ranged from 0.910 to 0.998 and 0.010 to 0.074 $cm^3\ cm^{-3}$, whereas the correlations and RMSE for the mixed soil moisture ranged from 0.996 to 0.998 and 0.007 to 0.010 $cm^3\ cm^{-3}$ (Table 8).

[43] Figures 9a–9d show the samples of unmixed $\theta(h)$ and $K(h)$ and $\theta(z,t)$ when the pixel-based soil moisture data are corrupted with errors while initial/boundary conditions are represented well [free drainage: initial condition $h(z,t=0) = -100$ cm], and when initial/boundary conditions are not represented well (groundwater level (GWL) = −200 cm) in the simulations. The reference soil-water retention and conductivity functions were closely matched by the solutions when the source of error in the modeling was from data alone (Figures 9a and 9b), since the soil hydraulic parameters were estimated reasonably well, as mentioned above. Some small discrepancies can be noticed at the wetter limb of s_2 soil-water retention curve possibly caused by the slight overestimation of α (note that bubbling pressure = $1/\alpha$) and in the drier end of s_3 [but these did not affect much the mixed soil hydraulic functions (not shown)]. Downscaled soil moisture under this scenario can be seen in Figure 10a. The impact of data errors is more manifested in the individual soil moisture series than in the mixed soil moisture (see Table 8). On the other hand, the combined effects of data errors and errors in initial and boundary conditions are more apparent in the individually derived soil hydraulic functions (Figures 9c and 9d); these compounded effects of data and modeling errors are translated to the relatively inferior matching of the downscaled soil moisture with the targets (Figure 10b).

3.2. Field Experiments and Validation

3.2.1. Field Scale

[44] The performance of the unmixing algorithm was tested using in situ soil moisture data observed during

Table 9. Performance of the Unmixing Solutions (Three Soils-One Vegetation) for WC11 During SMEX05 Campaign

	Statistics	
Categories	*R*	RMSE
(a) FD Bottom-Boundary Conditions		
Initial condition $h(z,t=0) = -100$ cm		
$s_{i=1,\ldots,3}v_1$	0.6542	0.0457
Initial condition $h(z,t=0) = -500$ cm		
$s_{i=1,\ldots,3}v_1$	0.6683	0.0488
Initial condition $h(z,t=0) = -1000$ cm		
$s_{i=1,\ldots,3}v_1$	0.6460	0.0459
(b) Variable Groundwater Conditions		
GWL = −100 cm; initial condition $h(z,t=0)$: equilibrium with initial GWL		
$s_{i=1,\ldots,3}v_1$	0.6237	0.0477
GWL = −150 cm; initial condition $h(z,t=0)$: equilibrium with initial GWL		
$s_{i=1,\ldots,3}v_1$	0.6327	0.0461
GWL = −200 cm; initial condition $h(z,t=0)$: equilibrium with initial GWL		
$s_{i=1,\ldots,3}v_1$	0.7394	0.0413
GWL = −250 cm; initial condition $h(z,t=0)$: equilibrium with initial GWL		
$s_{i=1,\ldots,3}v_1$	0.7385	0.0406
GWL = −300 cm; initial condition $h(z,t=0)$: equilibrium with initial GWL		
$s_{i=1,\ldots,3}v_1$	0.7389	0.0410
GWL = −390 cm; initial condition $h(z,t=0)$: equilibrium with initial GWL		
$s_{i=1,\ldots,3}v_1$	0.7064	0.0497

Table 10. [a]Sample Solution of the Unmixing Problem (Three Soils-One Vegetation) for WC11 During SMEX05 Campaign

Categories	Effective Soil Hydraulic Properties						Average Area Fraction ($s_i v_1$)	SD Area Fraction
	α	n	θ_{res}	θ_{sat}	K_{sat}	λ		
Variable Groundwater Conditions								
GWL = −250 cm; initial condition $h(z,t=0)$: equilibrium with initial GWL								
s_1	0.023	1.54	0.021	0.43	11.8	−0.950	0.587	0.111
s_2	0.018	1.56	0.012	0.42	44.9	−0.063	0.321	0.117
s_3	0.008	1.52	0.084	0.45	29.1	−0.001	0.092	0.036

[a]One of the best bottom-boundary conditions for WC11 field (see Table 9).

SMEX05 field campaign in Ames, Iowa. First, we calculated the daily average of the gridded in situ soil moisture data and then used the mixed time series for the unmixing analysis. Unlike in the idealized experiments where all sources of uncertainties can be controlled, applying the unmixing algorithm in actual field conditions is more challenging because of the incomplete information available about initial/boundary conditions, area soil proportions, and the like. The only good sources of information available at the time of the experiments were the time series of soil moisture data collected and the qualitative information about the soil and vegetation. For this reason, we conducted a sensitivity analysis on initial and boundary conditions while applying the unmixing algorithm (Table 3). The performances of these modeling conditions with respect to replicating the mixed time series of observed soil moisture are given in Table 9. Under free-drainage conditions, the R and RMSE of the solutions range from 0.65 to 0.67 and 0.046 to 0.049 $cm^3\ cm^{-3}$, respectively, whereas, under groundwater conditions, the R and RMSE of the solutions range from 0.62 to 0.74 and 0.041 to 0.050 $cm^3\ cm^{-3}$, respectively. By simple inference, the best modeling conditions for WC11 appear to be under groundwater conditions, 200–300 cm below the soil surface, as they produced time series of simulated (mixed) soil moisture that are highly correlated with the observed, and produced lesser errors. Table 10 shows the soil area-fraction statistics and respective effective soil hydraulic parameters estimated by the unmixing algorithm for WC11 field for modeling case under 250 cm groundwater depth. It shows that around 91% of the field is composed of soils 1 and 2, with soil3 comprising the rest (small fraction), and whose effective soil hydraulic properties are shown in Figure 11. Figure 11 also shows a validation of the derived unmixed soils and their mean soil hydraulic behavior compared with the typical hydraulic characteristics of the cataloged soils in WC11 reported in SSURGO (corresponding soil hydraulic parameters are derived from UNSODA [*Leij et al*., 1999]). During field survey, several locations in the WC11 field were sampled to measure actual soil hydraulic properties; we compared those data with the solutions from the unmixing experiments and those soil hydraulic properties of the cataloged soils. It is apparent that, in WC11 field, soils determined by the inverse modeling of observed soil moisture

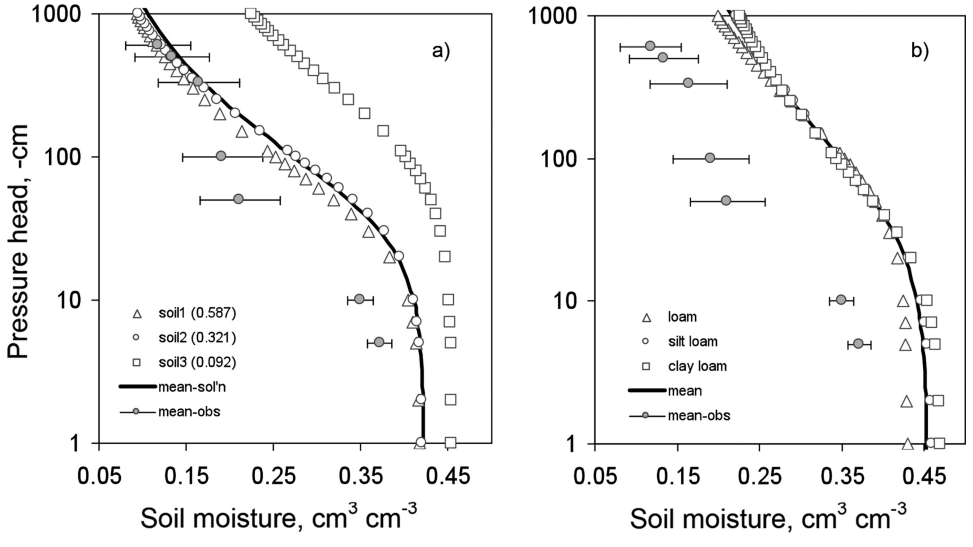

Figure 11. Sample results and validation of (a) unmixed soil-water retention curve, $\theta(h)$, compared with (b) cataloged soils in WC11 (three soils-one vegetation) during SMEX05. *Notes*: loam, silt loam, and clay loam are cataloged soils in this field; soil1, soil2, and soil3 are the corresponding solutions from the unmixing algorithm; mean-sol'n is the weighted retention curve from unmixing; mean is the average retention curve from the cataloged soils; mean-obs is the average soil hydraulic properties measured in the field. Error bars indicate one standard deviation. Area fractions are given in parentheses.

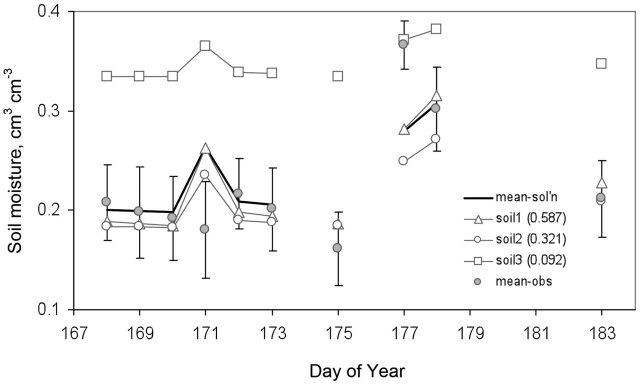

Figure 12. Sample results of unmixed and mixed soil moisture in WC11 field (three soils-one vegetation) during *SMEX05*. *Notes*: soil1, soil2, and soil3 are the corresponding solutions (unmixed) from the unmixing algorithm; mean-sol'n is the weighted soil moisture from unmixing; mean-obs is the average soil moisture measured in the field. Error bars indicate one standard deviation. Area fractions are given in parentheses.

appeared to behave closer with the measured soil hydraulic behavior of the field, suggesting further the value of mixed soil moisture (e.g., from RS) for inferring subgrid variability within a field. Figure 12 shows the unmixed and mixed soil moisture from the inverse modeling compared with the observations for modeling case under 250 cm groundwater depth. Interesting to note is the mismatch (direction) between measured and unmixed soil moisture on day-of-year 171. Soil moisture measurements were done across the WC11 field and thus captured the impact of a rainfall gradient, whereas SWAP used the rainfall data from a station (SCAN site) nearby the WC11 field. Subgrid rainfall variability could impact the results of the unmixing problem, which may be the reason of our mismatch in this case.

Table 11. Performance of the Unmixing Solutions Using ESTAR Soil Moisture for LW21 During SGP97 Campaign

Categories	Statistics	
	R	RMSE
(a) FD Bottom-Boundary Conditions		
Initial condition $h(z,t=0) = -100$ cm		
$\boldsymbol{s}_{i=1,\ldots,3},\mathrm{v}_{1,2}$	0.8988	0.0263
Initial condition $h(z,t=0) = -500$ cm		
$\boldsymbol{s}_{i=1,\ldots,3},\mathrm{v}_{1,2}$	0.9290	0.0249
Initial condition $h(z,t=0) = -1000$ cm		
$\boldsymbol{s}_{i=1,\ldots,3},\mathrm{v}_{1,2}$	0.9657	0.0160
(b) Variable Groundwater Conditions		
GWL $= -100$ cm; initial condition $h(z,t=0)$: equilibrium with initial GWL		
$\boldsymbol{s}_{i=1,\ldots,3},\mathrm{v}_{1,2}$	0.8288	0.0360
GWL $= -150$ cm; initial condition $h(z,t=0)$: equilibrium with initial GWL		
$\boldsymbol{s}_{i=1,\ldots,3},\mathrm{v}_{1,2}$	0.8565	0.0368
GWL $= -200$ cm; initial condition $h(z,t=0)$: equilibrium with initial GWL		
$\boldsymbol{s}_{i=1,\ldots,3},\mathrm{v}_{1,2}$	0.9045	0.0254

3.2.2. Airborne-RS *Scale*

[45] Validation experiments for the unmixing algorithm were also conducted using airborne-RS data (ESTAR) during SGP97 at LW21 site. As in the case of the field-scale experiments, we have also performed sensitivity analysis of modeling conditions for LW21 (Table 3), and, based on the performance of these modeling conditions, we selected the best condition for the site. Because of the time-saving schemes included in the unmixing algorithm and the use of micropopulations in GA, the sensitivity analysis did not take a long time to perform. However, if one knows the bottom-boundary condition of the study domain, this part can be skipped. Table 11 shows that most of the modeling conditions used resulted in high performance with R ranging from 0.82 to 0.96 and RMSE from 0.016 to 0.037 $\mathrm{cm}^3\ \mathrm{cm}^{-3}$ (between simulated mean and ESTAR soil moisture). It appears however that a free-draining bottom boundary, with drier initial condition [$h(z,t=0) = -1000$ cm], gave the best results, whose estimated effective soil hydraulic parameters and soil-vegetation area-fraction statistics are given in Table 12. Figure 13 shows a comparison between the measured soil hydraulic properties of LW21 and those by the unmixing algorithm and cataloged soils from SSURGO (soil hydraulic parameters deduced from UNSODA [*Leij et al*., 1999]). Unlike with the case of WC11 field, where cataloged soil hydraulic property estimates did not match well with the observations, in LW21 they matched reasonably well (Figure 13b). On the other hand, the estimates from the unmixing algorithm also matched well with the measurements especially for soils 2 and 3 and the resultant soil hydraulic behavior (Figure 13a). Soil1 appears to be an outlier but is composed only of 16.6% of the area compared with the approximately 83.4% covered by soils 2 and 3. The role of soil1 however should not be downplayed, as shown in the validation of soil moisture simulations (Figure 14). It appears that soil1 served to capture the outer envelopes of the soil moisture dynamics in LW21, based on the unmixing algorithm.

4. Concluding Remarks and Recommendations

[46] The unmixing method presented here could provide a quick way to estimate area fractions of soils and potentially vegetations and subgrid effective soil hydraulic properties within a pixel from large-scale soil moisture measurements, crucial for accounting subgrid variability in large-scale hydrologic models. Land surface models often require fractions of soils within the control volume as inputs. However, the combined SVAT-GA unmixing method could only extract subgrid soil moisture/soil properties and soil-vegetation fractions in the pixel and cannot pinpoint where they are in the pixel. To apply the method to downscale large-scale spaceborne RS soil moisture, a stagewise downscaling procedure is possibly needed; first, downscaling with a deterministic method (spatially explicit) then the unmixing algorithm will narrow-down possible soil moisture subgrid variability. Accounting subgrid variability in hydrologic modeling can improve the simulation of fluxes [*Crow and Wood*, 2002; *Crow et al*., 2005].

[47] Testing and evaluation of the unmixing algorithm under idealized conditions showed that the method could

Table 12. Sample Solution[a] of the Unmixing Problem (Three Soils-Two Vegetations) Using ESTAR Soil Moisture for LW21 During SGP97 Campaign

	Effective Soil Hydraulic Parameters						Vegetation 1, v_1 (Grass)		Vegetation 2, v_2 (Wheat)	
Categories	α	n	θ_{res}	θ_{sat}	K_{sat}	λ	Average Area Fraction ($s_i v_1$)	SD Area Fraction	Average Area Fraction ($s_i v_2$)	SD Area Fraction
FD Bottom-Boundary Conditions										
Initial condition $h(z,t=0) = -1000$ cm										
s_1	0.061	2.05	0.012	0.32	45.8	0.35	0.159	0.018	0.007	0.026
s_2	0.012	1.48	0.060	0.40	12.4	−0.36	0.670	0.098	0.068	0.062
s_3	0.025	1.34	0.067	0.38	15.0	−1.11	0.095	0.066	0.001	0.003

[a]Best bottom-boundary condition for LW21 field (see Table 11).

extract exact values of soil hydraulic properties and area fractions of soils and vegetations under different hydroclimatic conditions assuming a perfect prognosis, even with complex soil-vegetation combinations. Data and modeling errors could impact to the quality of the unmixing results. With appropriate modeling conditions, the unmixing results faired well with our reference data considering moderate error in soil moisture data. The combined errors in modeling conditions and data could lead to less than ideal results.

[48] The unmixing method was tested and validated under field conditions, using both in situ soil moisture and airborne-based RS measurements in selected sites under two contrasting hydroclimatic regions, Iowa and Oklahoma. In WC11 field (Iowa), where in situ (field-average) soil moisture was used in the inverse modeling, the unmixed soil hydraulic properties appeared to match better with the measurements compared with the typical soil hydraulic properties of soils cataloged in the study area. In LW21 site (Oklahoma), where airborne-based soil moisture data were used in the inverse modeling, both the unmixed and cataloged soil hydraulic properties behaved reasonably well with measurements. In both validation sites, majority of the unmixed soil moisture series were honored within the envelope of soil moisture measurements.

[49] In the sensitivity analyses, we observed the sensitivity of area fractions with modeling conditions. To account for this source of uncertainty, a consensus modeling could be done [e.g., *Ines and Mohanty*, 2009]. Future validation studies should include other sources of subgrid variability, e.g., topography and rainfall variability, and should also include more soils in the pixel and extend to irrigated areas. These validations should test the caveats of the current study. Because of the limited scope of the validation conducted in this study, we could not fully show that the more complex the subgrid variability is, the more sensitive the micro-GA would be to errors in grid-averaged soil moisture observations and to errors in other required model inputs (e.g., climate, irrigation, and model parameters); of particular interest to test would be on the variability of area fractions extracted by GA. The unmixing method should be

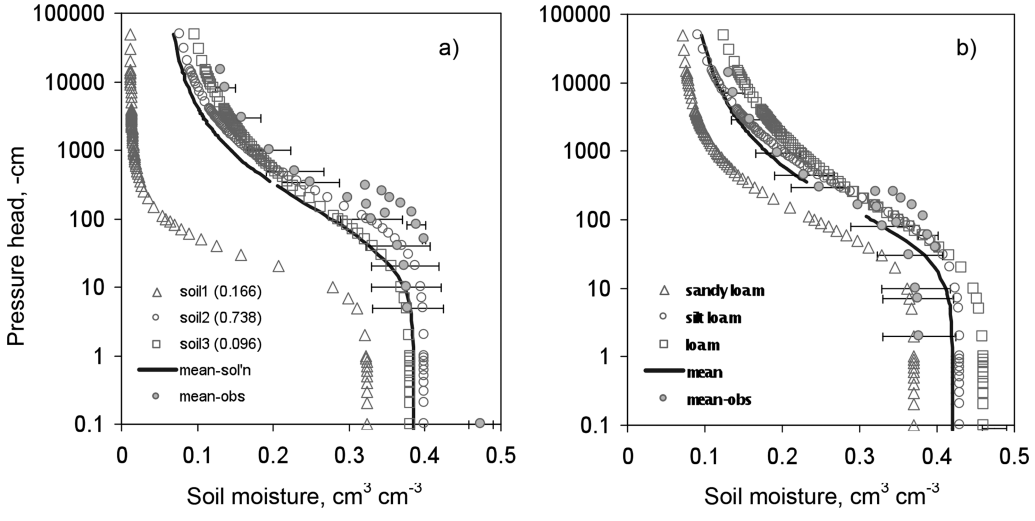

Figure 13. Sample results and validation of (a) unmixed soil-water retention curve, $\theta(h)$, compared with (b) cataloged soils in LW21 (three soils-two vegetations) during SGP97. *Notes*: sandy loam, silt loam, and loam are cataloged soils in this field; soil1, soil2, and soil3 are the corresponding solutions from the unmixing algorithm; mean-sol'n is the weighted retention curve from unmixing; mean is the average retention curve from the cataloged soils; mean-obs is the average soil hydraulic properties measured in the field. Error bars indicate one standard deviation. Area fractions are given in parentheses.

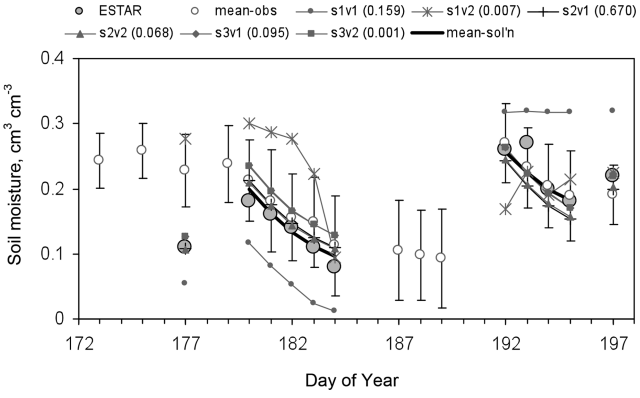

Figure 14. Sample results of unmixed and mixed soil moisture in LW21 field (three soils-one vegetation) during *SGP97*. *Notes*: $s_{\#}v_{\#}$ are the corresponding solutions (unmixed) from the unmixing algorithm; mean-sol'n is the weighted soil moisture from unmixing; mean-obs is the average soil moisture measured in the field. ESTAR is the soil moisture from airborne RS. Error bars indicate one standard deviation. Area fractions are given in parentheses.

tested in terms of fine-scale soil moisture estimates as well, aside from grid-averaged soil moisture.

[50] **Acknowledgments.** This research was funded by NASA THP (NNX08AF55G and NNX09AK73G) grants. We like to acknowledge the partial support of NSF (CMG/DMS grants CMG-06-21113 and DMS-09-34837) for this work. We thank N. N. Das of the Department of Biological and Agricultural Engineering, Texas A&M University (now at NASA-JPL), for collating the in situ data used in this study. Part of the work of first author was supported by NOAA cooperative agreement grant NA05OAR4311004. Finally, we thank the editors and reviewers for their valuable comments and suggestions.

References

Bartalis, Z., V. Naeimi, S. Hasenauer, and W. Wagner (2008), ASCAT soil moisture product handbook, *ASCAT Soil Moisture Rep. Ser. 15*, Inst. of Photogramm. and Remote Sens., Vienna Univ. of Technol., Austria.

Belmans, C., J. G. Wesseling, and R. A. Feddes (1983), Simulation of water balance of a cropped soil: SWATRE, *J. Hydrol.*, *63*, 271–286.

Brantley, S. L., et al. (2006), Frontiers in exploration of the critical zone: Report of a workshop sponsored by the National Science Foundation (NSF), 30 pp., Newark, Del., 24–26 Oct., 2005.

Cai, X., D. C. McKinney, and L. S. Lasdon (2001), Solving nonlinear water management models using a combined genetic algorithm and linear programming approach, *Adv. Water Resour.*, *24*, 667–676.

Carroll, D. L. (1998), GA Fortran Driver version 1.7, CU Aerospace, IL. [Available at http://www.cuaerospace.com/carroll/ga.html.]

Carsel, R. F., and R. S. Parrish (1988), Developing joint probability-distributions of soil-water retention characteristics, *Water Resour. Res.*, *24*, 755–769.

Chan-Hilton, A. B., and T. B. Culver (2000), Constraint handling for genetic algorithms in optimal remediation design, *J. Water Resour. Plan. Manage*, *126*(3), 128–137.

Cieniewski, S. E., J. W. Eheart, and S. Ranjithan (1995), Using genetic algorithms to solve a multi-objective groundwater monitoring problem, *Water Resour. Res.*, *31*, 399–409.

Crow, W. T., and E. F. Wood (2002), The value of coarse-scale soil moisture observations for regional surface energy balance modeling, *J. Hydrometeorol.*, *3*, 467–482.

Crow, W. T., D. Ryu, and J. S. Famiglietti (2005), Upscaling of field-scale soil moisture measurements using a distributed land surface model, *Adv. Water Resour.*, *28*, 1–14, doi:10.1016/j.advwatres.2004.10.004.

Das, N. N., and B. P. Mohanty (2006), Root zone soil moisture assessment using remote sensing and vadose zone modeling, *Vadose Zone J.*, *5*, 296–307.

Das, N. N., D. Entekhabi, and E. G. Njoku (2011), An algorithm for merging SMAP radiometer and radar data for high-resolution soil moisture retrieval, *IEEE Trans. Geosci. Remote Sens.*, *49*, 1504–1512.

Droogers, P., Bastiaanssen, W. G. M., Beyazgül, M., Kayam, Y., Kite, G. W., and H. Murray-Rust(2000), Distributed agro-hydrological modeling of an irrigation system in Western Turkey, *Agric. Water Manage.*, *43*, 183–202.

Entekhabi, D., et al. (2010), The Soil Moisture Active Passive (SMAP) mission, *Proc. IEEE*, *98*, 704–716.

Ferreira, M. E., L. G. Ferreira, E. E. Sano, and Y. E. Shimabukuro (2007), Spectral linear mixture modelling approaches for land cover mapping of tropical savanna areas in Brazil, *Int. J. Remote Sens.*, *28*, 413–429.

Goldberg, D. E. (1989), *Genetic Algorithms in Search and Optimization and Machine Learning*, Addison-Wesley, Washington, D. C.

Goldberg, D. E. (2002), *The Design of Innovation: Lessons From and for Competent Genetic Algorithms*, Kluwer Acad., Norwell, Mass.

Holben, B. N., and Y. E. Shimabukuro (1993), Linear mixing applied to coarse spatial resolution data from multispectral satellite sensors, *Int. J. Remote Sens.*, *14*, 2231–2240.

Holland, J. H. (1975), *Adaptation in Natural and Artificial Systems*, Univ. of Mich. Press, Ann Arbor.

Hollinger, S. E., and S. A. Isard (1994), A soil moisture climatology of Illinois, *J. Clim.*, *7*, 822–833.

Ines, A. V. M., and P. Droogers (2002), Inverse modeling in estimating soil hydraulic functions: A genetic algorithm approach, *Hydrol. Earth Syst. Sci.*, *6*(1), 49–65.

Ines, A. V. M., and K. Honda (2005), On quantifying agricultural and water management practices from low spatial resolution RS data using genetic algorithms: A numerical study for mixed-pixel environment, *Adv. Water Resour.*, *28*, 856–870.

Ines, A. V. M., and B. P. Mohanty (2008a), Parameter conditioning with a noisy Monte Carlo genetic algorithm to estimate effective soil hydraulic properties from space, *Water Resour. Res.*, *44*, W08441, doi:10.1029/2007WR006125.

Ines, A. V. M., and B. P. Mohanty (2008b), Near-surface soil moisture assimilation to quantify effective soil hydraulic properties using genetic algorithm: 1. Conceptual modeling, *Water Resour. Res.*, *44*, W06422, doi:10.1029/2007WR005990.

Ines, A. V. M., and B. P. Mohanty (2008c), Near-surface soil moisture assimilation to quantify effective soil hydraulic properties under different hydro-climatic conditions, *Vadose Zone J.*, *7*, 39–52.

Ines, A. V. M., and B. P. Mohanty (2009), Near-surface soil moisture assimilation for quantifying effective soil hydraulic properties using genetic algorithm: 2. With air-borne remote sensing during SGP97 and SMEX02, *Water Resour. Res.*, *45*, W01408, doi:10.1029/2008WR007022.

Ines, A. V. M., K. Honda, A. D. Gupta, P. Droogers, and R. S. Clemente (2006), Combining remote sensing-simulation modeling and genetic algorithm optimization to explore water management options in irrigated agriculture, *Agric. Water Manage.*, *83*, 221–232.

Jackson, T. J., D. M. Le Vine, T. J. Schmugge, and F. R. Schiebe (1995), Large area mapping of soil moisture using ESTAR passive microwave radiometer in Washita '92, *Remote Sens. Environ.*, *53*, 27–37.

Jackson, T. J., D. M. Le Vine, A. Y. Hsu, A. Oldak, P. J. Starks, C. T. Swift, J. D. Isham, and M. Haken (1999), Soil moisture mapping at regional scales using microwave radiometry: The Southern Great Plains hydrology experiment, *IEEE Trans. Geosci. Remote Sens.*, *37*, 2136–2151.

Jackson, T. J., R. Bindlish, M. Cosh, A. Gasiewski, B. Stankov, M. Klein, B. Weber, and V. Zavorotny (2005a), Soil moisture experiments 2004 (SMEX04) polarimetric scanning radiometer, AMSR-E and heterogeneous landscapes, *Int. Geosci. Remote Sens. Symp.*, *2*, 1114–1117, Art. 1525311.

Jackson, T. J., R. Bindlish, A. J. Gasiewski, B. Stankov, M. Klein, E. G. Njoku, D. Bosch, T. L. Coleman, C. Laymon, and P. J. Starks (2005b), Polarimetric scanning radiometer C and X band microwave observations during SMEX03, *IEEE Trans. Geosci. Remote Sens.*, *43*, 2418–2430.

Kerr, Y., P. Waldteufel, J.-P. Wigneron, J.-M. Martinuzzi, J. Font, and M. Berger (2001), Soil moisture retrieval from space: The Soil Moisture and Ocean Salinity (SMOS) mission, *IEEE Trans. Geosci. Remote Sens.*, *39*, 1729–1735.

Krishnakumar, K. (1989), Micro-genetic algorithms for stationary and non-stationary function optimization, in *SPIE: Intelligent Control and Adaptive Systems*, vol. 1196, pp. 289–296, Philadelphia, Pa.

Leij, F. J., W. J. Alves, M. Th. Van Genuchten, and J. R. Williams (1999), The UNSODA unsaturated soil hydraulic database, in *Characterization*

and Measurement of the Hydraulic Properties of Unsaturated Porous Media, edited by M. Th. Van Genuchten, F. J. Leij, and L. Wu, pp. 1269–1281, Univ. of Calif., Riverside, Calif.

Merlin, O., J. P. Walker, A. Chehbouni, and Y. Kerr (2008), Towards deterministic downscaling of SMOS soil moisture using MODIS derived soil evaporative efficiency, *Remote Sens. Environ.*, *112*, 3935–3946.

Michalewicz, Z. (1996), *Genetic Algorithms + Data Structures = Evolution Programs*, 3rd ed. rev. and extended ed., Springer, London, U. K.

Mohanty, B. P., P. J. Shouse, D. A. Miller, and M. T. Van Genuchten (2002), Soil property database: Southern Great Plains 1997 hydrology experiment, *Water Resour. Res.*, *38*(5), 1047, doi:10.1029/2000WR000076.

Mualem, Y. (1976), A new model for predicting the hydraulic conductivity of unsaturated porous media, *Water Resour. Res.*, *12*, 513–522.

Ni-Meister, W., Houser, P. R., and J. P. Walker (2006), Soil moisture initialization for climate prediction: Assimilation of scanning multifrequency microwave radiometer soil moisture data into a land surface model, *J. Geophys. Res.*, *111*, D20102, doi:10.1029/2006JD007190.

Njoku, E. G., T. L. Jackson, V. Lakshmi, T. Chan, and S. V. Nghiem (2003), Soil moisture retrieval from AMSR-E, *IEEE Trans. Geosci. Remote Sens.*, *41*, 215–229.

Ritzel, B., J. W. Eheart, and S. Ranjithan (1994), Using genetic algorithms to solve multi-objective groundwater pollution containment problem, *Water Resour. Res.*, *30*, 1589–1603.

Robock, A., K. Y. Vinnikov, G. Srinivasan, J. K. Entin, S. E. Hollinger, N. A. Speranskaya, S. Liu, and A. Namkhai (2000), The global soil data bank, *Bull. Am. Meteorol. Soc.*, *81*, 1281–1299.

Sarwar, A., W. G. M. Bastiaanssen, M. Th. Boers, and J. C. Van Dam (2000), Evaluating drainage design parameters for the fourth drainage project, Pakistan by using SWAP model: Part I—Calibration, *Irrig. Drain. Syst.*, *14*, 257–280.

Schaap, M. G., F. J. Leij, and M. Th. Van Genuchten (1999), A bootstrap-neural network approach to predict soil hydraulic parameters, in *Proceedings of the International Workshop, Characterization and Measurements of the Hydraulic Properties of Unsaturated Porous Media*, edited by M. Th. Van Genuchten, F. J. Leij, and L. Wu, pp. 1237–1250, Univ. of Calif., Riverside, Calif.

Scott, C. A., W. G. M. Bastiaanssen, and A. Mobin-ud-Din (2003), Mapping root zone soil moisture using remotely sensed optical imagery, *J. Irrig. Drain. Eng.*, *129*(5), 326–335, doi:10.1061/(ASCE)0733-9437(2003)129:5(326).

Shimabukuro, Y. E., and J. A. Smith (1991), The least-squares mixing models to generate fraction images derived from remote sensing multispectral data, *IEEE Trans. Geosci. Remote Sens.*, *29*, 16–20.

Singh, R., J. G. Kroes, J. C. Van Dam, and R. A. Feddes (2006a), Distributed ecohydrological modelling to evaluate the performance of irrigation system in Sirsa district, India: I. Current water management and its productivity, *J. Hydrol.*, *329*, 692–713.

Singh, R., J. G. Kroes, J. C. Van Dam, and R. A. Feddes (2006b), Distributed ecohydrological modelling to evaluate irrigation system performance in Sirsa district, India: II. Impact of viable water management scenarios, *J. Hydrol.*, *329*, 714–723.

Tateishi, R., Y. Shimazaki, and P. D. Gunin (2004), Spectral and temporal linear mixing model for vegetation classification, *Int. J. Remote Sens.*, *25*, 4203–4218.

Van Dam, J. C. (2000), Field-scale water flow and solute transport. SWAP model concepts, parameter estimation and case studies, Ph.D. dissertation, Wageningen Univ., Netherlands.

Van Dam J. C., J. Huygen, J. G. Wesseling, R. A. Feddes, P. Kabat, P. E. V. Van Waslum, P. Groenendijk, and C. A. Van Diepen (1997), Theory of SWAP version 2.0: Simulation of water flow and plant growth in the soil–water–atmosphere–plant environment, *Tech. Doc. 45*, Wageningen Agric. Univ. and DLO Winand Staring Cent., Netherlands.

Van Genuchten, M. Th. (1980), A closed-form equation foe predicting the hydraulic conductivity of unsaturated soils, *Soil Sci. Soc. Am. J.*, *44*, 892–898.

Wang, D., and X. Cai (2007), Optimal estimation of irrigation schedule—An example of quantifying human interferences to hydrologic processes, *Adv. Water Resour.*, *30*, 1844–1857.

Wesseling, J. G., and J. G. Kroes (1998), A global sensitivity analysis of the model SWAP, *Rep. 160*, DLO Winand Staring Cent., Wageningen, Netherlands.

Wösten, J. H. M., G. H. Veerman, and J. Stolte (1994), Water retention and hydraulic conductivity functions of top- and subsoils in the Netherlands: The Staring series, 66 pp., *Tech. Doc. 18*, Winand Staring Cent., Wageningen, Netherlands.

Wösten, J. H. M., A. Lilly, A. Nemes, and C. Le Bas (1999), Development and use of a database of hydraulic properties of European soils, *Geoderma*, *90*, 169–185.